Angewandte Chemie
Eine Zeitschrift der Gesellschaft Deutscher Chemiker

Supporting Information

An Efficient Conjugation Approach for Coupling Drugs to Native Antibodies via the Pt^{II} Linker *Lx* for Improved Manufacturability of Antibody–Drug Conjugates

Eugen Merkul, Joey A. Muns, Niels J. Sijbrandi, Hendrik-Jan Houthoff, Bart Nijmeijer, Gerro van Rheenen, Jan Reedijk, and Guus A. M. S. van Dongen*

anie_202011593_sm_miscellaneous_information.pdf

Author Contributions

E.M. Conceptualization: Lead; Data curation: Lead; Formal analysis: Lead; Investigation: Lead; Methodology: Equal; Project administration: Lead; Supervision: Lead; Visualization: Lead; Writing—original draft: Lead; Writing—review & editing: Lead
J.M. Data curation: Lead; Formal analysis: Equal; Investigation: Supporting; Methodology: Equal; Validation: Supporting; Visualization: Supporting; Writing—review & editing: Supporting
N.S. Data curation: Supporting; Methodology: Supporting; Validation: Supporting; Writing—review & editing: Supporting
H.H. Conceptualization: Supporting; Funding acquisition: Lead; Investigation: Supporting; Resources: Lead
B.N. Data curation: Supporting; Formal analysis: Supporting; Validation: Supporting
G.v. Conceptualization: Supporting; Funding acquisition: Lead; Investigation: Supporting; Resources: Lead
J.R. Writing—review & editing: Supporting; literature search: Supporting
G.v. Conceptualization: Supporting; Funding acquisition: Supporting; Investigation: Supporting; Methodology: Supporting; Resources: Supporting; Writing—original draft: Supporting; Writing—review & editing: Supporting.

Supporting Information

Content:

1. Materials and methods 3
   - 1.1. Materials 3
   - 1.2. Cell lines 3
   - 1.3. Analytical methods 3
     - 1.3.1. Analytical RP-HPLC 3
     - 1.3.2. SEC 3
     - 1.3.3. SEC-MS 4
     - 1.3.4. SDS-PAGE 4
     - 1.3.5. Nanodrop UV 4
     - 1.3.6. pH 4
     - 1.3.7. Binding assay 4
     - 1.3.8. iTLC 4
     - 1.3.9. *In vitro* cell viability assay 5
   - 1.4. Biodistribution 5

2. The initial *Lx*-conjugation procedure 5
   - 2.1. The initial *Lx*-conjugation procedure applied to Cl-*Lx*-DFO (**1a**) 5
   - 2.2. The initial *Lx*-conjugation procedure applied to Cl-*Lx*-AF (**1f**) 6

3. Optimization of the *Lx*-conjugation reaction 7
   - 3.1. General information on the optimization study 7
   - 3.2. Determination of the conjugation efficiency 8
   - 3.3. Screening of the conjugation buffers/pH 8
   - 3.4. Addition of organic co-solvents 10
   - 3.5. Addition of inorganic salts 13
     - 3.5.1. Screening of anions 13
     - 3.5.2. Screening of cations 15
   - 3.6. Addition of amino acids, amino acid derivatives, and other additives 16
   - 3.7. Fine-tuning of the Cl-*Lx* (**1a**) stoichiometry in the conjugation reaction 19
   - 3.8. Screening of the conjugation temperature and time 21
   - 3.9. Pre-activation of Cl-*Lx* (**1a**) by iodide exchange 22
   - 3.10. The effect of the TU quenching step on the conjugation efficiency 24
   - 3.11. The buffer exchange from the Herceptin® formulation buffer 26
   - 3.12. Conjugation with various mAbs 29
   - 3.13. Conjugation of semi-final complexes bearing different halido leaving groups 31
   - 3.14. Screening of the reaction molarity 38

4. Comparison of *Lx*-conjugates **2a** and **2b** obtained via the initial and the optimized *Lx*-conjugation procedures applied to Cl-*Lx*-DFO-Fe(III) (**1a**) 39
   - 4.1. Synthesis of DFO based *Lx*-conjugates **2a** and **2b** using the initial and the optimized *Lx*-conjugation methods from Cl-*Lx*-DFO-Fe(III) (**1a**) 40
     - 4.1.1. Milligram scale synthesis of *Lx*-conjugate **2a** 40
     - 4.1.2. Milligram scale synthesis of *Lx*-conjugate **2b** 40
   - 4.2. Immunoreactive antibody fraction after the *Lx*-conjugation 40

4.3. Comparison of the serum stability of *Lx*-conjugates **^{89}Zr-2a** and **^{89}Zr-2b** 41
4.4. Comparison of the pharmacokinetics of *Lx*-conjugates **^{89}Zr-2a** and **^{89}Zr-2b** 41

5. Comparison of *Lx*-conjugates **3a** and **3b** obtained via the initial and the optimized *Lx*-conjugation procedures applied to Cl-*Lx*-AF (**1f**) 42
5.1. Synthesis of auristatin F based *Lx*-conjugates **3a** and **3b** from Cl-*Lx*-AF (**1f**) using the initial and the optimized *Lx*-conjugation methods 43
5.1.1. Milligram scale synthesis of *Lx*-conjugate **3a** 43
5.1.2. Milligram scale synthesis of *Lx*-conjugate **3b** 43
5.2. Comparison of DAR and payload distribution 43
5.3. *In vitro* efficacy of auristatin F based *Lx*-conjugates **3a** and **3b** 44

6. The formulation stability study of the lead *Lx*-ADC trastuzumab-*Lx*-AF (**3b$_{stab}$**) 44
6.1. The conjugation procedure, formulation, and storage conditions 45
6.2. The stability study 45

7. The multigram scale synthesis of the lead *Lx*-ADC trastuzumab-*Lx*-AF (**3c**) from I-*Lx*-AF (**1g**) using the optimized *Lx*-conjugation procedure 46

7.1. The multigram scale synthesis of the semi-final complex I-*Lx*-AF (**1g**) 46
7.2. The multigram scale synthesis of trastuzumab-*Lx*-AF (**3c**) from I-*Lx*-AF (**1g**) using the optimized *Lx*-conjugation method 46
7.2.1. The multigram scale *Lx*-conjugation procedure 46
7.2.2. Quenching with TU 47
7.2.3. Purification by diafiltration 47
7.3. Quality control (QC) of trastuzumab-*Lx*-AF (**3c**) produced on a multigram scale using the optimized *Lx*-conjugation method 48
7.3.1. Protein content by Nanodrop UV 49
7.3.2. Monomeric purity by SEC 49
7.3.3. Protein composition by SDS-PAGE 49
7.3.4. Unbound TU-*Lx*-AF (**1h**) by HPLC 50
7.3.5. DAR by SEC-MS 51
7.3.6. Potency by CTB-based bioassay 52

8. References 53

1. Materials and methods

1.1. Materials

All starting reagents and solvents were obtained from commercial providers and used without further purification, unless otherwise stated. Most important chemicals and their providers are following: sodium iodide (Sigma), HEPES (Sigma), PBS (Fresenius Krabi), thiourea (Sigma), *L*-histidine (Sigma), *L*-histidine × HCl × H_2O (Sigma), *D*-(-)-trehalose dihydrate (Sigma), polysorbate 20 (TWEEN 20, Merck), DMA (Sigma). Desferal® (DFO; also called deferoxamine or desferrioxamine) was obtained from the Amsterdam UMC (location VUmc) hospital pharmacy. ^{89}Zr (≥ 0.15 GBq/nmol in 1 mol/L oxalic acid) was obtained from Cyclotron BV, Amsterdam. Water was distilled and deionized (18 MΩ/cm) by means of a milli-Q water filtration system (Millipore, USA).

Trastuzumab (Herceptin®), cetuximab, rituximab, ofatumumab, and obinutuzumab were obtained from the Amsterdam UMC (location VUmc) hospital pharmacy. For the multigram scale synthesis of trastuzumab-*Lx*-auristatin F (**3c**) (auristatin F will be abbreviated with AF) and the milligram scale reference *Lx*-conjugates (**3c$_{ref}$**) (section 7.), the trastuzumab biosimilar (BS) was obtained from Swiss Biotech Center (SBC).

Cl-*Lx*-DFO-Fe(III) (**1a**) and Cl-*Lx*-AF (**1f**) were prepared as described in [1] N. J. Sijbrandi *et al.*, *Cancer Res.* **2017**, *77*, 257-267. I-*Lx*-AF × 2.0 TFA × 2.5 NaI (**1g**) was manufactured by ChemConnection/Ardena, as described in [2] Merkul *et al.*, *Green Chem.* **2020**, *22*, 2203-2212.

1.2. Cell lines

Cell lines used were the breast cancer lines MDA-MB-231, JIMT-1, BT-474, and SK-BR-3, the ovarian cancer cell line SK-OV-3, and the gastric cancer cell line NCI-N87. JIMT-1 was obtained from DSMZ on August 25, 2014, after cytogenetic testing by the supplier, and used within 6 months after resuscitation. MDA-MB-231, NCI-N87, SK-OV-3, BT-474, and SK-BR-3 were obtained from the ATCC United Kingdom on August 25, 2014, after cytogenetic testing by the supplier, and used within 6 months after resuscitation. Cytogenetic testing was not repeated by us. However, all cell lines were controlled by us for primary growth characteristics (morphology and growth rate) and HER2 expression before use in experiments. MDA-MB-231 is a HER2-negative cell line; SK-BR-3, BT-474, SK-OV-3, and NCI-N87 are overexpressing HER2; JIMT-1 is developed from tumor cells of a patient with trastuzumab resistance and is HER2-positive.[3]

1.3. Analytical methods

1.3.1. Analytical RP-HPLC

Analytical RP-HPLC was performed using a Jasco HPLC system, equipped with a PU-2089Plus pump, an MD-2015Plus detector, and an AS-2057Plus autoinjector, using an Alltima C18 5µ column (4.6 × 250 mm) and linear gradients of MeCN/H_2O + 0.1% TFA.

1.3.2. SEC

SEC was performed using a Jasco HPLC system equipped with a PU-2089Plus pump, an MD-2015Plus detector, and an AS-2057Plus autoinjector using a Sepax Zenix-C SEC-300 column (300 Å, 7.8 × 300 mm) (Sepax Technologies Inc., Newark, DE, USA). The sample (20 µL) was injected using a mixture of 0.05

mol/L sodium phosphate, 0.15 mol/L sodium chloride (pH 6.8), and 0.01 mol/L NaN_3 as the eluent at a flow rate of 1 mL/min.. The antibody integrity was defined as the percentage of monomeric mAb peak area at 280 nm of the total protein area at 280 nm.

1.3.3. SEC-MS

SEC-MS analysis was performed using a Thermo Finnigan LC system (Thermo Finnigan, San Jose, CA, USA) coupled to a Bruker Q-TOF mass spectrometer (Bremen, Germany) equipped with an electrospray ionization (ESI) source. A Zenix-C column (4.6 × 300 mm; 5 µm; Sepax Technologies Inc., Newark, DE, USA) was used. The mobile phase consisted of a mixture of H_2O, MeCN, TFA, and formic acid (79.9/19.9/0.1/0.1, v/v/v/v, respectively). A 17-min. isocratic run was performed at a flow rate of 350 µL/min.. A sample (10 µL) was injected. The LC flow was directed to the MS source from 2 to 10 min. using the switch valve present on the mass spectrometer. The rest of the solvent flow was directed to waste to prevent source contamination. MS analysis was done in positive ionization mode using the following settings: ESI voltage, 4.5 kV; dry gas temperature, 190 °C; dry gas flow rate, 8 L/min.; nebulizer pressure, 1.6 bar; in-source collision-induced dissociation energy, 120 eV; ion energy, 5 eV; collision cell energy, 15 eV. Data was analyzed using Bruker Daltonics Data Analysis software. Protein ion charge assignment and molecular mass determinations were performed using the "Charge Deconvolution" utility of the Data Analysis software.

1.3.4. SDS-PAGE

SDS-PAGE was performed on a Phastgel System (GE Healthcare Life Sciences) using pre-formed 7.5% SDS-PAGE gels under reducing and non-reducing conditions. A sample (5 µL) was diluted with PBS (5 µL) and SDS-PAGE sample buffer (10 µL) and gels were analyzed by isotope counting using a phosphorimager and quantified with ImageQuant software.

1.3.5. Nanodrop UV

The protein contents were determined using a Nanodrop NanoVue Plus (GE; Biochrom Spectrophotometers 28943212; Serial No. 117232). The absorption at 280 nm was measured and the protein concentration was calculated using dilutions of trastuzumab (Herceptin®) with a known concentration as calibration standards.

1.3.6. pH

pH of buffers used and of the reaction mixtures were measured using a BioTrode (Hamilton, 238140) coupled to an SI Analytics (SI Analytics, Lab 865) system for read-out.

1.3.7. Binding assay

Binding characteristics of *Lx*-ADCs were determined in an immunoreactivity assay, essentially as described by [4] Lindmo *et al., J. Immunol. Methods* **1984**, *72*, 77-89, using a serial dilution of 2% paraformaldehyde-fixed SK-OV-3 cells and a fixed amount of radiolabeled *Lx*-conjugates ^{89}**Zr-2a** and ^{89}**Zr-2b**. After overnight incubation at 4 °C, the cell suspension was centrifuged and the specific binding was calculated as the percentage of cell-bound radioactivity relative to the total amount of radioactivity in the assay. This was corrected for non-specific binding, as determined with a 500-fold excess of non-radioactive trastuzumab. All binding assays were performed in triplicate.

1.3.8. iTLC

Instant thin layer chromatography (iTLC) analysis of ADCs was carried out to assess their radiochemical purity. Silica-impregnated glass fiber sheets (PI Medical Diagnostic Equipment BV) were used with 20

mmol/L citrate buffer (pH 5.0)/MeOH (3/7) as the mobile phase. As readout for ^{89}Zr counting, a gamma-well counter (Wallac LKB-CompuGamma 1282; Pharmacia) was used.

1.3.9. *In vitro* cell viability assay

Cell-Titer Blue (CTB)-based *in vitro* cytotoxicity bioassay was performed as described in [1] N. J. Sijbrandi *et al., Cancer Res.* **2017**, *77*, 257-267.

1.4. Biodistribution

Animal experiments as part of this research project have been conducted at VUmc. All animal experiments were authorized due to a permit of the VUmc as license holder to (1) breed animals, (2) receive animals from approved commercial suppliers and (3) use animals in licensed research projects with (4) accredited animal facilities based on a permit of the 'Nederlandse Voedsel- en Warenautoriteit' as responsible governmental authority. (5) All personnel involved in animal experiments is approved by the Animal Welfare Body VU and VUmc based on personal licenses (certificates) including competences requiring internal training. All animal experiments conducted for this manuscript have been approved by the 'Centrale Commissie Dierproeven' (Central Commission for Animal Experiments) of the Netherlands Government under permit number AVD114002016510 for Prof. Dr. Guus A.M.S. van Dongen at VUmc. All experiments have been performed according to the Netherlands Law on Animal Research (Wet op Dierproeven) in full agreement with the Directive 2010/63/EU with local approval by and under supervision of the Animal Welfare Body VU and VU Medical Center.

The biodistribution of constructs **3a** and **3b** was evaluated in nude mice. 12 female mice (HSD:Athymic Nude-Foxn1nu, 21-31 g [Harlan]; 8-10 weeks old at the time of the experiments) were anesthetized by inhalation of 2% isoflurane and injected intravenously via the retroorbital plexus with the radiolabeled constructs in a 100 µL injection volume. Blood was collected via the tail 2 h, 24 h, and 48 h after injection of the tracer. At the end of the experiment, 72 h after injection, the mice were anesthetized, bled, sacrificed, and dissected. After blood, tumor, and healthy tissues had been weighed, the amount of radioactivity in each sample was measured in a γ-counter for ^{89}Zr activity. Radioisotope uptake was calculated as the percentage of the injected dose per gram of tissue (%ID).

2. The initial *Lx*-conjugation procedure

2.1. The initial *Lx*-conjugation procedure applied to Cl-*Lx*-DFO (1a)

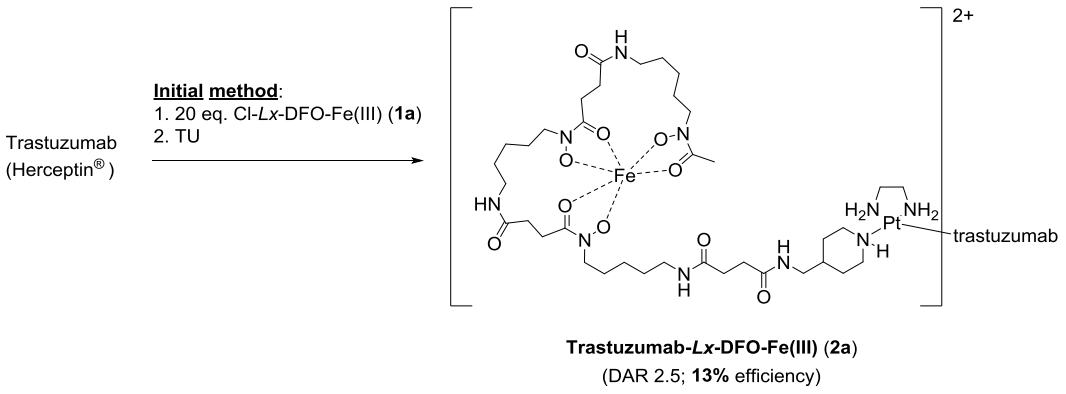

Scheme S1. The initial *Lx*-conjugation with DFO-Fe(III) as a payload.

The laboratory milligram scale synthesis of the chlorido semi-final complex Cl-*Lx*-DFO-Fe(III) (**1a**) and the initial conjugation procedure yielding trastuzumab-*Lx*-DFO-Fe(III) (**2a**) were described in [1] N. J. Sijbrandi *et al.*, *Cancer Res.* **2017**, *77*, 257-267.

Conjugation procedure (initial method): In a 1.5 mL screw cap Eppendorf tube, Cl-*Lx*-DFO-Fe(III) (**1a**) (Cl-*Lx*; 147 µL of a ~5 mM solution, ~20 eq.) was added to a solution of trastuzumab (Herceptin®; 5.0 mg, 238 µL of a 21 mg/mL solution, 1.0 eq.) in tricine buffer (41.2 µL of a 200 mM solution, pH 8.5) and incubated in a thermoshaker at 37 °C for 24 h. Then, TU (426 µL of a 20 mM solution; final concentration 10 mM) was added to the mixture that was incubated at 37 °C for 30 min. After that, the mixture was purified using a spin filter (MWCO = 30 kDa; 15 mL, washed 4 × with PBS buffer), after which it was reconstituted to 1.5 mL. The product **2a** was obtained as a ~5 mg/mL solution in PBS. DAR: 2.5 (as determined by SEC-MS).

This conjugation was used as a starting point for the in section 3. described optimization, using the same semi-final complex, Cl-*Lx*-DFO-Fe(III) (**1a**).

2.2. The initial *Lx*-conjugation procedure applied to Cl-*Lx*-AF (1f)

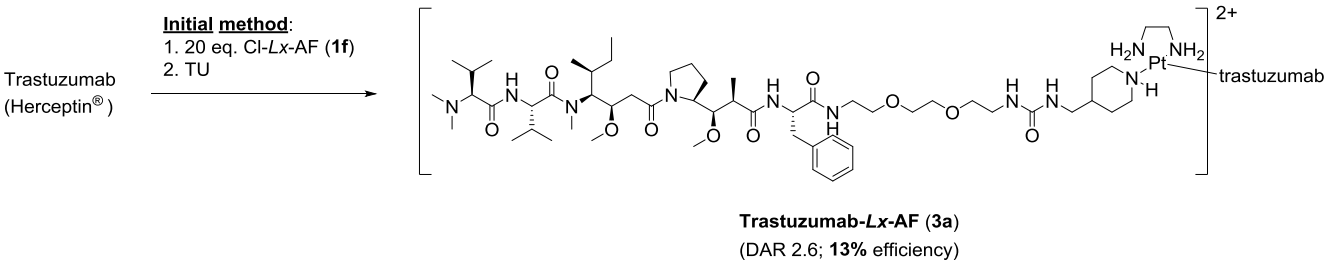

Scheme S2. The initial *Lx*-conjugation with AF as a payload.

The laboratory milligram scale synthesis of the chlorido semi-final complex Cl-*Lx*-AF (**1f**) and the initial conjugation procedure yielding trastuzumab-*Lx*-AF (**3a**) were described in [1] N. J. Sijbrandi *et al.*, *Cancer Res.* **2017**, *77*, 257-267.

Conjugation procedure (initial method): In a 1.5 mL screw cap Eppendorf tube, Cl-*Lx*-AF (**1f**) (204.1 µL of a ~5 mM solution in 10 mM NaCl/DMA 9:1, ~20 eq.) was added to a solution of trastuzumab (Herceptin®; 7.5 mg, 357.0 µL of a 21 mg/mL solution, 1.0 eq.) in tricine buffer (62.8 µL of a 200 mM solution, pH 8.5) and incubated in a thermoshaker at 37 °C for 24 h. Then, TU (623.9 µL of a 20 mM solution; final concentration 10 mM) was added to the mixture that was incubated at 37 °C for 30 min. After that, the mixture was purified using a spin filter (MWCO = 30 kDa; 15 mL, washed 4 × with PBS buffer), after which it was reconstituted to 1.5 mL. The product **3a** was obtained as a 4.74 mg/mL solution in PBS (determined by Nanodrop UV). DAR: 2.6 (as determined by SEC-MS).

3. Optimization of the *Lx*-conjugation reaction

3.1. General information on the optimization study

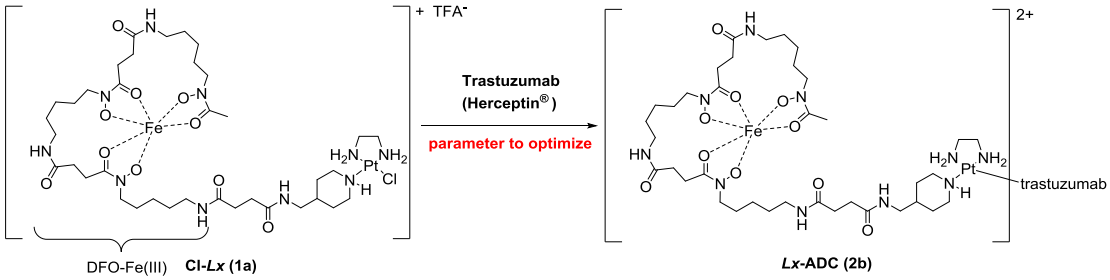

Scheme S3. General scheme describing the optimization of the *Lx*-conjugation.

For this optimization work, a Desferal® (DFO) based model semi-final complex Cl-*Lx*-DFO-Fe(III), "Cl-*Lx*", (**1a**) and trastuzumab (Herceptin®) as a mAb were chosen.

Compound **1a** has the following advantages that make it a valuable model compound for the intended optimization studies (described in [1] N. J. Sijbrandi *et al.*, *Cancer Res.* **2017**, *77*, 257-267): (i) its absorption maximum at 430 nm allows to determine the conjugation efficiency by SEC without purification of the conjugation mixtures, thus allowing a high throughput screening, (ii) as a payload, it behaves similarly to our lead candidate in terms of reactivity and distribution over the antibody surface, (iii) Fe(III) can be easily replaced by the radioisotope ^{89}Zr(IV),[16] making *in vitro* cell assays and *in vivo* biodistribution experiments possible for validation of the conjugate characteristics, and (iv) the conjugates with this payload are stable in human serum as well as in the storage buffer.

The synthesis of compound Cl-*Lx* (**1a**) was described in [1] N. J. Sijbrandi *et al.*, *Cancer Res.* **2017**, *77*, 257-267. Cl-*Lx* (**1a**) was used as a 20 mM solution in NaCl for the conjugation experiments; it was stored in the freezer at -18 °C. No significant loss of purity was observed upon storage (> 1 year).

The following reaction parameters were screened:

- conjugation buffers/pH (section 3.3.)
- addition of organic co-solvents (section 3.4.)
- addition of inorganic salts (section 3.5.)
- addition of amino acids, amino acid derivatives, and other additives (section 3.6.)
- adjustment of *Lx*-stoichiometry (section 3.7.)
- conjugation temperature and time (section 3.8.)
- influence of pre-activation of semi-final precursors (section 3.9.)
- the effect of the TU quenching step (section 3.10.)
- buffer exchange of Herceptin® (section 3.11.)
- conjugation with various mAbs (section 3.12.)
- influence of the halido leaving ligand of the semi-final precursors (section 3.13.)
- reaction molarity (section 3.14.)

To find optimal conjugation conditions, the results of a screening of each parameter were directly used in a subsequent screening experiment, unless stated otherwise.

3.2. Determination of the conjugation efficiency

The conjugation efficiency in these optimization experiments was determined as the percentage of the ultraviolet-visible (UV-Vis) spectroscopy peak area of conjugated DFO-Fe(III) of the total DFO-Fe(III) UV peak area, *i.e.* [a/a% (DFO-Fe(III))$_{conjugated}$ / a/a% (DFO-Fe(III))$_{conjugated+unconjugated}$] × 100%, as measured by size-exclusion high-performance liquid chromatography (SE-HPLC) at 430 nm (Fig. S1).

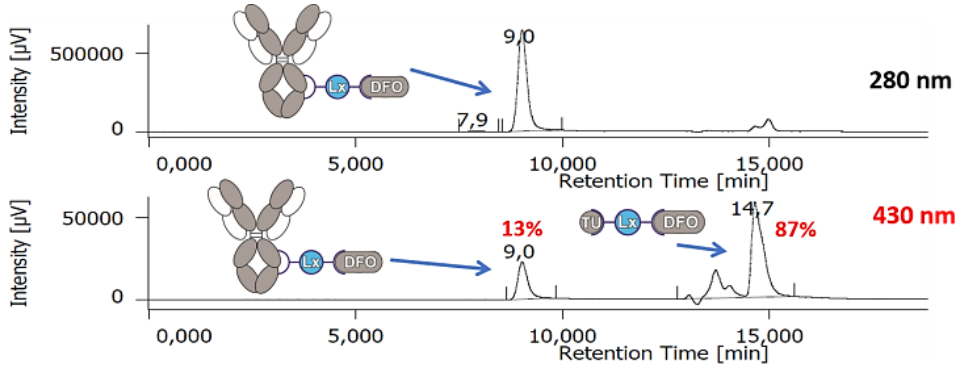

Figure S1. Determination the of conjugation efficiency by SE-HPLC, shown for the initial conjugation conditions.

3.3. Screening of the conjugation buffers/pH

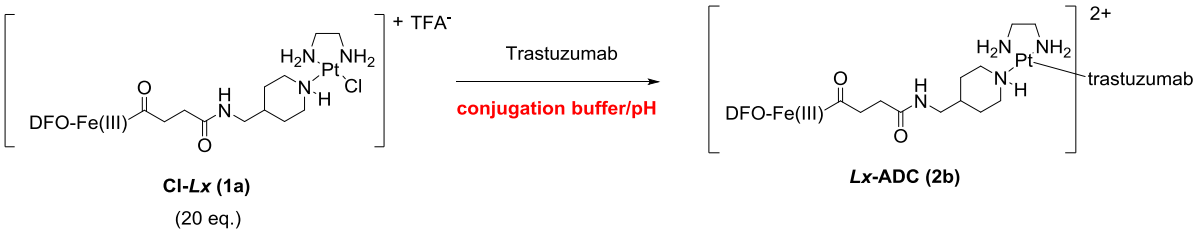

Scheme S4. Screening of the conjugation buffers/pH.

Performed screening experiments are summarized in Tables S1, S2, and S3.

Conjugation procedure: Trastuzumab in its native clinical formulation and Cl-*Lx* (**1a**) (20 eq.) were incubated in different buffers (Table S1) at 37 °C for 24 h. After the conjugation followed by treatment with a solution of thiourea (TU; 10 mM final concentration), the mixture was analyzed by SEC to determine the conjugation efficiency (Fig. S2).

Table S1. Buffer and pH optimization (pH range 2.7-10.4).

Entries	Buffer	Buffer concentration (mM)	Buffer pH range
1-5	phosphate	20	6.0-8.0
6-7	tricine	20	8.0-8.5
8-11	carbonate	20	9.0-10.4
12-21	citric acid/Na_2HPO_4	20	2.7-7.3

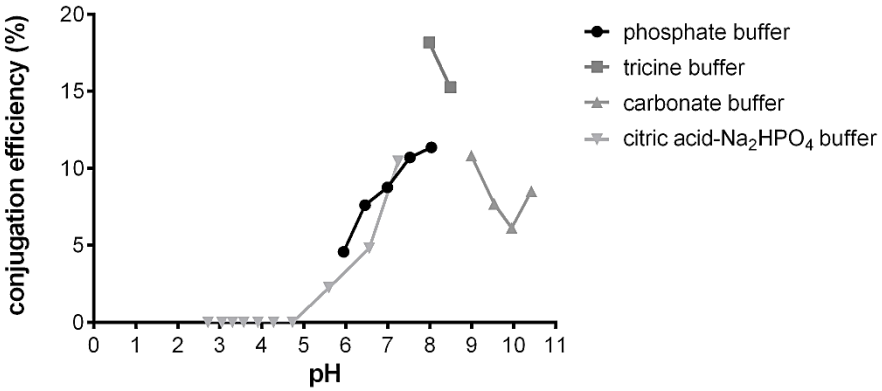

Figure S2. Optimization of buffer and pH (2.7-10.4).

No conjugation was observed in the conjugation buffers with low pH values (pH range 2.7-5.0); this is in line with our hypothesis that conjugation is mainly directed towards His (typical pKa of 5.5-7.5). On the other hand, a significant increase in antibody aggregation and formation of smaller peptide fragments (antibody degradation) was observed in SEC chromatograms at high pH values (carbonate buffers range 9.0-10.4). Thus, the optimal pH range was found to be between pH 7.0-8.5. The best result was obtained for the conjugation in a 20 mM tricine buffer at a pH of 8.0, resulting in **18%** conjugation efficiency.

To find the optimal buffer pH, the pH range was narrowed to 6.9-8.7. For this experiment, 5 HEPES buffers (pH range 6.9-8.1) and 5 tricine buffers (pH range 7.6-8.7) were used (Table S2).

Table S2. Buffer and pH optimization (pH range 6.9-8.7).

Entries	Buffer	Buffer concentration (mM)	Buffer pH range
22-31	HEPES	20	6.9-8.1
32-41	tricine	20	7.6-8.7

The results obtained with tricine buffers (Fig. S3) indicate a pH optimum at 8.0 (efficiency of **18%**); at higher pH values, the conjugation efficiency started to decrease. Conjugations in the HEPES buffers showed a minor improvement compared to tricine buffers: the optimal HEPES buffer of pH 8.1 delivered a conjugation efficiency of **21%**.

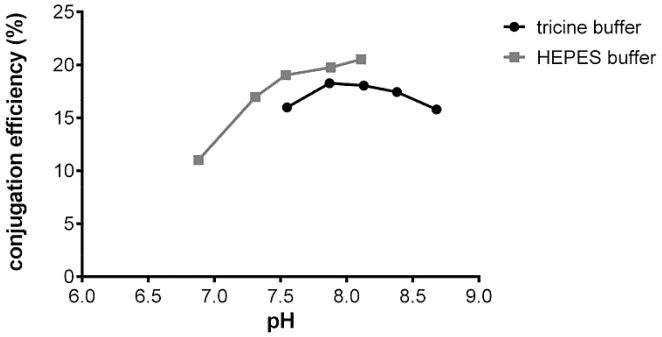

Figure S3. Optimization of buffer and pH (6.9-8.7).

To determine if there is a buffer concentration optimum, the optimal buffer (HEPES; pH 8.1) was used in a 1-100 mM concentration range (Table S3).

Table S3. Optimization of the concentration range of HEPES.

Entries	Buffer	Buffer concentration range (mM)	Buffer pH
42-51	HEPES	1-100	8.11

An increase in the HEPES buffer concentration does not have a significant effect on the conjugation efficiency (Fig. S4). A plateau of the maximal conjugation efficiency (~**20%**) was reached at ~10 mM buffer concentration, probably because at lower concentrations the pH of the conjugation mixture becomes lower due to the native formulation buffer of trastuzumab (for more details on this point, see section 3.11.).

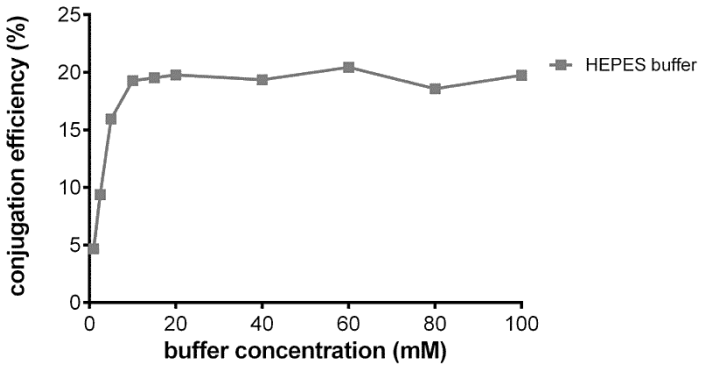

Figure S4. Effect of concentration of the HEPES buffer.

It appeared that the *Lx*-conjugation reaction is mainly influenced by the pH value and not by the nature of the buffer (in the absence of *Lx*-reactive components in the buffers; see *e.g.* section 3.11.).

3.4. Addition of organic co-solvents

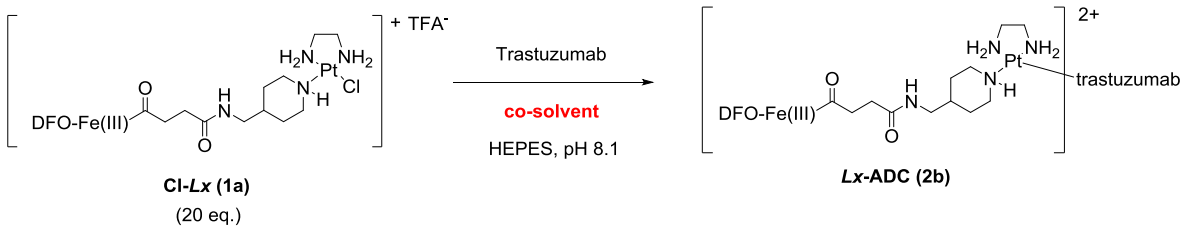

Scheme S5. Screening of organic co-solvents in the *Lx*-conjugation mixture.

Generally, organic co-solvents are often used in bioconjugation reactions of small molecules with proteins to increase the solubility of a payload in an aqueous solution where the conjugation reaction takes place. On the other hand, such co-solvents can be disadvantageous for the integrity of a protein. The positive charge which is present at the Pt(II) center in our semi-final complexes **1** – the substrates of the conjugation

reaction – increases the hydrophilicity of small molecules compared to non-*Lx* containing drug-linker constructs. However, depending on the payload it can still be necessary to add a co-solvent to dissolve the *Lx*-payload molecule. Moreover, the semi-final complexes **1** can contain some residual solvents from their production step. Therefore, a broad solvent screening was performed to investigate: (i) if addition of organic co-solvents would benefit the *Lx*-conjugation efficiency, (ii) which co-solvents can be used in the conjugation reaction without loss of the integrity of an antibody, and (iii) if there are co-solvents which have a negative effect on the *Lx*-conjugation and thus need to be avoided during the manufacturing step or in the formulation of the semi-final complexes **1**. This last reason is important *e.g.* in situations in which a co-solvent is needed to dissolve the *Lx*-payload compound **1**.

Performed screening experiments are summarized in Table S4.

Conjugation procedure: Trastuzumab in its native clinical formulation and Cl-*Lx* (**1a**) (20 eq.) were incubated in HEPES, pH 8.1 with the addition of different organic co-solvents (Table S5) at 37 °C for 24 h. After the conjugation followed by treatment with a solution of TU, the mixture was analyzed by SEC to determine the conjugation efficiency (Fig. S5).

Table S4. Co-solvents (compound and concentration).

Entries	Buffer	Buffer concentration (mM)	Buffer pH	Organic co-solvent	Co-solvent concentration (% v/v)
55-56	HEPES	20	8.1	none	0
57-83	HEPES	20	8.1	see Table S5	5
84-90	HEPES	20	8.1	see Table S5	10

Solvents were preferably selected according to three criteria: they should (i) be miscible with water, at least in the concentration range used, (ii) preferentially be green,[5] and (iii) cover various classes of organic compounds to discover possible additional non-solubility related effects (Table S5).

Table S5. List of co-solvents used in the optimization screening.

Solvent class	Co-solvent	Category according to the Pfizer solvent guide[5] (unless cited otherwise)	Boiling point (°C)	Solubility in water (g/100g)
Alcohols	methanol	green	65	miscible
	ethanol	green	78	miscible
	1-propanol	green	97	miscible
	2-propanol	green	82	miscible
	1-butanol	green	117	6.3
	isobutanol	green	108	7.0
	tert-amyl alcohol	not mentioned	102	12
	ethylene glycol	yellow	197	miscible
	glycerin	green[6]	290	miscible
Ethers	tetrahydrofuran (THF)	yellow	66	30
	2-methyl-THF (2-MeTHF)	yellow	79	14
	1,2-dimethoxyethane (DME)	red	85	miscible
	1,4-dioxane	red	101	miscible
Ketones	acetone	green	56	miscible
	2-butanone (methyl ethyl ketone, MEK)	green	80	27.5

Amides/nitriles	dimethylformamide (DMF)	red	153	miscible
	dimethylacetamide (DMA)	red	165	miscible
	acetonitrile	yellow	82	miscible
Esters	ethyl lactate	green	153	miscible
	ethyl acetate	green	145	8.7
	methyl acetate	yellow[6]	57	24.4
Sulfur containing	dimethylsulfoxide (DMSO)[a]	yellow	189	25.3
	dimethylsulfon ($DMSO_2$)[b]	-	238	15.0

[a] DMSO was only used for the sake of completeness since it is strongly discouraged to be used in combination with Pt(II).[7] [b] $DMSO_2$ (mp 109 °C; used industrially as a high-temperature solvent) was included because of its structural similarity to DMSO without the ability of coordinate to Pt(II) via the *S*-atom.

The results are summarized in Fig. S5.

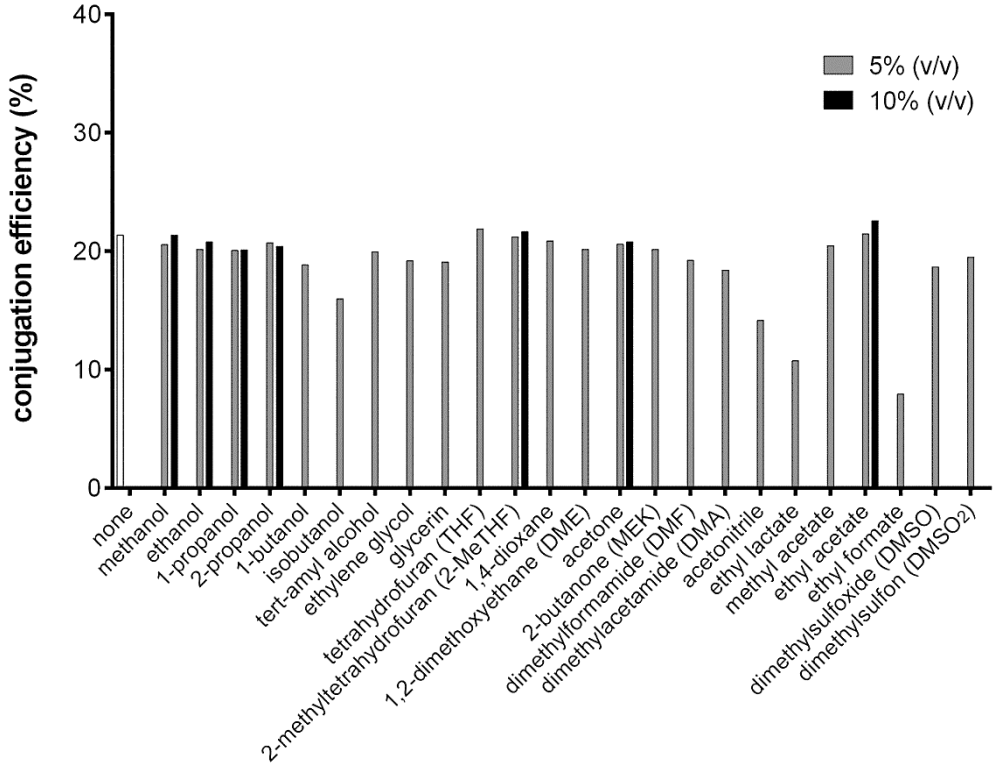

Figure S5. Effect of organic co-solvents on the conjugation efficiency.

It was found that none of the tested organic co-solvents improved the *Lx*-conjugation. On the other hand, solvents such as alcohols, ethers, acetone, *N*,*N*-dimethylformamide (DMF), *N*,*N*-dimethylacetamide (DMA), and ethyl acetate did not affect/harm the *Lx*-conjugation reaction and thus can be safely used in the production, purification or formulation steps of the precursor semi-final complexes **1**. The observation that *N*,*N*-dimethylacetamide (DMA) did not affect the conjugation efficiency is especially important since the semi-final complexes **1** are often formulated in aqueous solutions containing 10 vol% of DMA.

Another conclusion from this experiment is that use of acetonitrile should be avoided. Most likely due to competing coordination of this co-solvent to Pt(II), the conjugation efficiency had decreased from ~21% to ~14%. This observation is of importance since acetonitrile was used as an eluent component during the purification of the semi-final complexes **1** – substrates of the conjugation reaction – by preparative HPLC on a laboratory scale. Consequently, acetonitrile was replaced by methanol as an eluent component.

3.5. Addition of inorganic salts

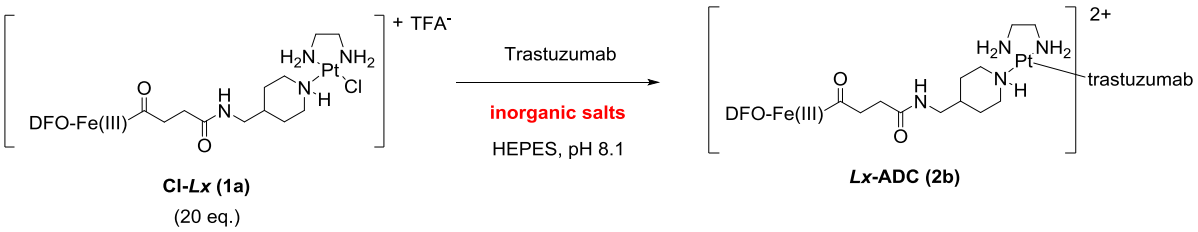

Scheme S6. Screening of inorganic salt additives.

3.5.1. Screening of anions

Performed screening experiments are summarized in Table S6.

Conjugation procedure: Trastuzumab in its native clinical formulation and Cl-*Lx* (**1a**) (20 eq.) were incubated in HEPES, pH 8.1 with the addition of different sodium salts (Table S7) at 37 °C for 24 h. After the conjugation followed by treatment with a solution of TU, the mixture was analyzed by SEC to determine the conjugation efficiency (Fig. S6).

Table S6. Addition of sodium salts.

Entry	Buffer	Buffer concentration (mM)	Buffer pH	Additional salt in the buffer	Additional salt concentration (mM)
91-113	HEPES	20	8.1	see Table S7	30

The screened sodium salts (Table S7) were used at a 30 mM concentration for the initial screening, and positive hits were later screened for an optimal concentration. *Note*: NaCl was also always present in the conjugation mixtures (concentration was ~6.5 mM) resulting from the formulation of the Cl-*Lx* (**1a**) stock solution (5 mM in 20 mM NaCl) that was used for this screening.

Table S7. Sodium salts used for the anion screening.

Sodium salt	Chemical sum formula
sodium fluoride	NaF
sodium chloride	NaCl
sodium bromide	NaBr
sodium iodide	NaI
sodium iodate	$NaIO_3$
sodium nitrate	$NaNO_3$
sodium perchlorate	$NaClO_4$
sodium sulfate	Na_2SO_4
sodium mesylate	NaOMs
sodium triflate	NaOTf
sodium tosylate	NaOTs
sodium tetrafluoroborate	$NaBF_4$
sodium hexafluorophosphate	$NaPF_6$

sodium formate	HCOONa
sodium acetate	CH_3COONa
sodium trifluoroacetate	CF_3COONa
sodium pentafluoropropionate	C_2F_5COONa

The results of this screening are depicted in Fig. S6 (also Fig. 2 of the main part of the manuscript).

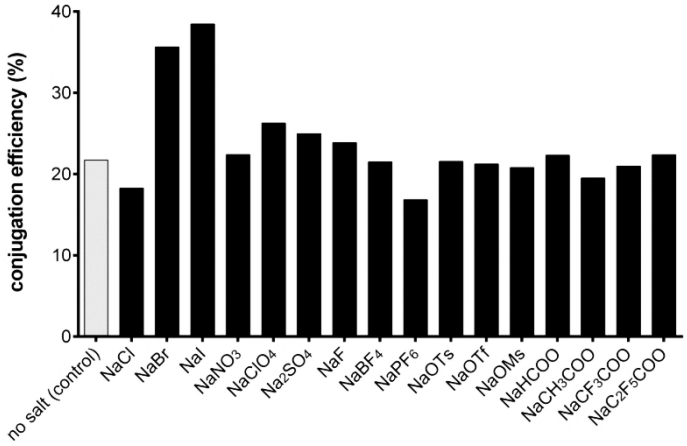

Figure S6. The results of the anion screening.

To investigate the influence of the concentration of the two "magic salts", NaBr and NaI in detail, the concentration range of the best salt NaI and of the second-best salt NaBr, both in a 0-100 mM concentration range, were tested (Table S8).

Table S8. Screening of different concentrations of NaBr and NaI.

Entries	Buffer	Buffer concentration (mM)	Buffer pH	Additional salt	Additional salt concentration range (mM)
114-122	HEPES	20	8.1	NaI	0-100
123-130	HEPES	20	8.1	NaBr	0-100

The results (Fig. S7) showed that even at the lowest concentration (1 mM) NaI significantly increased the conjugation efficiency (from ~20% to ~**35%**). Since the Cl-*Lx* (**1a**) is present in excess compared to NaI in this conjugation reaction (NaI: complex **1a** = 1:1.6), it seems that NaI has a catalytic effect in *Lx*-conjugations. Further, the conjugation efficiency was found to be quite constant over a broad range of NaI concentrations (ranging from ~10 to 100 mM), with only a slight decrease at high NaI concentration.

NaBr showed an increasing curve of the conjugation efficiencies in the concentration range 0-50 mM and the same efficiencies at 50 mM and 100 mM. This can be explained by a less efficient formation of the bromido complex **1b** intermediate compared to the formation of the corresponding iodido complex **1c** intermediate.

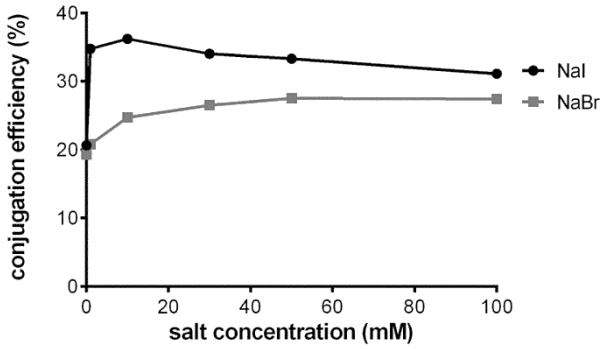

Figure S7. Effect of different concentrations of the best salt additives NaI and NaBr.

3.5.2. Screening of cations

Various iodide salts were tested to determine if their cations also show an effect on the conjugation efficiency and possibly to find an iodide salt that would further improve the conjugation efficiency. Besides, it was important to demonstrate that all the iodide sources, *i.e.* all the formulations that can release an iodide anion *in situ* during the conjugation, can be used as promoters for the conjugation, or if some salts are prohibited from use in the *Lx*-conjugations. To this end, conjugations were performed using the iodide salts including M^+, M^{2+}, M^{3+}, and M^{4+} as well as organic cations; all salts were used at a 10 mM concentration (Table S9). Additionally, three bromide salts (NaBr, KBr, and LiBr) were also tested.

Conjugation procedure: Trastuzumab in its native clinical formulation and Cl-*Lx* (**1a**) (20 eq.) were incubated in HEPES, pH 8.1 with the addition of different iodide salts (Table S9) and bromide salts (*vide infra*) at 37 ^{o}C for 24 h. After the conjugation followed by treatment with a solution of TU, the mixture was analyzed by SEC to determine the conjugation efficiency (Fig. S8).

Table S9. Iodide salts used for the cation screening.

Iodide salt	Chemical sum formula
sodium iodide	NaI
potassium iodide	KI
lithium iodide	LiI
cesium iodide	CsI
rubidium iodide	RbI
ammonium iodide	NH_4I
magnesium iodide	MgI_2
calcium iodide	CaI_2
strontium iodide	SrI_2
zinc iodide[a]	ZnI_2
manganese iodide	MnI_2
aluminium iodide	AlI_3
indium iodide	InI_3
germanium iodide	GeI_4
guanidinium iodide	CH_6N_3I
tetramethyl ammonium iodide	$(CH_3)_4NI$
acetylcholine iodide (AChI)	$C_7H_{16}NO_2I$
5-(2-hydroxyethyl)-3,4-dimethylthiazolium iodide	$C_7H_{12}NOSI$
trimethylsulfoxonium iodide	$(CH_3)_3SOI$

[a] ZnI_2 caused solubility problems and an antibody aggregation of ~30%; therefore, the results with this salt were not included in Fig. S8.

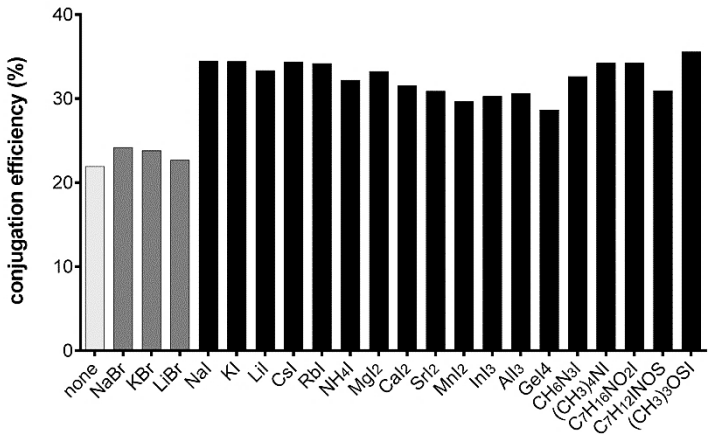

Figure S8. The results of the cation screening.

The results showed no significant influence of tested cations on the conjugation efficiency (Fig. S8).

3.6. Addition of amino acids, amino acid derivatives, and other additives

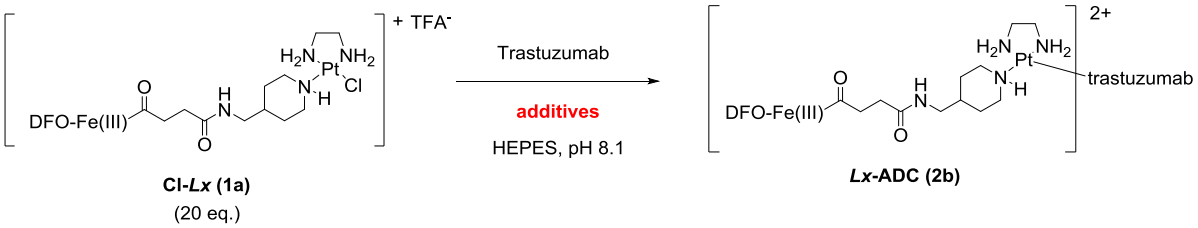

Scheme S7. Screening of various additives.

Performed screening experiments are summarized in Tables S10 and S12.

Conjugation procedure: Trastuzumab in its native clinical formulation and Cl-*Lx* (**1a**) (20 eq.) were incubated in HEPES (NaI was present (Table S10) or absent during these experiments (Table S12)), pH 8.1 with the addition of different additives (Table S11) at 37 ^{o}C for 24 h. After the conjugation followed by treatment with a solution of TU, the mixture was analyzed by SEC to determine the conjugation efficiency (Fig. S9).

Table S10. Conjugation reaction with various additives.

Entry	Buffer	Buffer concentration (mM)	Buffer pH	Additional salt in the buffer	Additional salt concentration (mM)	Additive	Additive concentration (mM)
152-166	HEPES	20	8.1	NaI	10	see Table S11	30

Table S11. Screening of additives.

Additive	Remarks
imidazole	*N*-Heterocyclic core of *L*-His
***L*-His**	Amino acid containing an *N*-heterocycle (imidazole core) which is able to coordinate to *Lx*. It is the amino acid to which *Lx* is conjugated (*e.g.* 26 His residues are found in trastuzumab). Present in the trastuzumab formulation buffer (each Herceptin® vial contains 440 mg trastuzumab, 9.9 mg *L*-His × HCl, and 6.4 mg *L*-His)
***L*-Lys**	Amino acid containing an NH_2 group potentially able to coordinate to *Lx*. It is abundant in trastuzumab (96 Lys residues)
***L*-Arg**	Amino acid containing a guanidine group potentially able to coordinate to *Lx*
***L*-Cys**	Amino acid containing a free thiol group able to coordinate to *Lx* (not present in reduced form in the native trastuzumab)
***DL*-Met**	Amino acid containing a thioether group able to coordinate to *Lx*
seleno-*DL*-Met	Amino acid containing a selenoether group able to coordinate to *Lx* (not present in trastuzumab)
acetyl-*L*-Met amide	Mimics Met residues in antibodies
acetyl-*L*-His amide	Mimics His residues in antibodies
TWEEN® 20 (polysorbate 20)	Emulsifier used in the trastuzumab formulation buffer
trehalose dihydrate guanosine	Disaccharide used in the trastuzumab formulation buffer in a large quantity *N*7 of this nucleoside has a high affinity to Pt(II). It is the preferred binding site for cisplatin *in vivo*

Amino acids *L*-His (a crucial amino acid since it is present in the formulation buffer of Herceptin® (trastuzumab); it has therefore always been present in the *Lx*-conjugation mixtures), *L*-Lys, *L*-Arg, *L*-Cys, *DL*-Met, and seleno-*DL*-Met were selected as additives because they contain functional groups that are potentially able to coordinate to Pt(II). From previous experiments we concluded that conjugation of *Lx* can take place on His (an *N*-heterocycle), Met (a thioether), and Cys (a thiol) residues of proteins. Since no cysteines in the reduced form are present in native antibodies, these can be ruled out as a possible binding site. Met-Pt(II) bonds are thermodynamically less stable and kinetically labile. They can be cleaved by TU,[8] so that the corresponding Met-adducts are removed during the TU quenching/washing step after the conjugation (*vide infra*). Therefore, we consider coordination to His residues to be crucial for the *Lx*-conjugation which is supported by various (yet indirect) evidences. Despite the unstable binding characteristics of Met and the absence of reduced Cys in native antibodies, their role as an additive in the conjugation reactions can be interesting since Pt(II) is known to have a high affinity for sulfur donors.

Next to the amino acids, also protected (on both the amino and the carboxylic acid groups) amino acids acetyl-*L*-His amide and acetyl-*L*-Met amide that directly mimic the amino acid residues of an antibody were tested.

Moreover, imidazole was used as a heterocyclic core structure of *L*-His. Further, Tween® 20 (polysorbate 20) was tested because this emulsifier is used in the trastuzumab formulation buffer. For the same reason, trehalose dihydrate, a disaccharide present in large quantity in the formulation buffer of trastuzumab, was tested as an additive. Moreover, since *N*7 of guanosine is known to have a high affinity for Pt(II) – in fact, it is the major binding site of cisplatin *in vivo* –, this purine nucleoside was also tested.

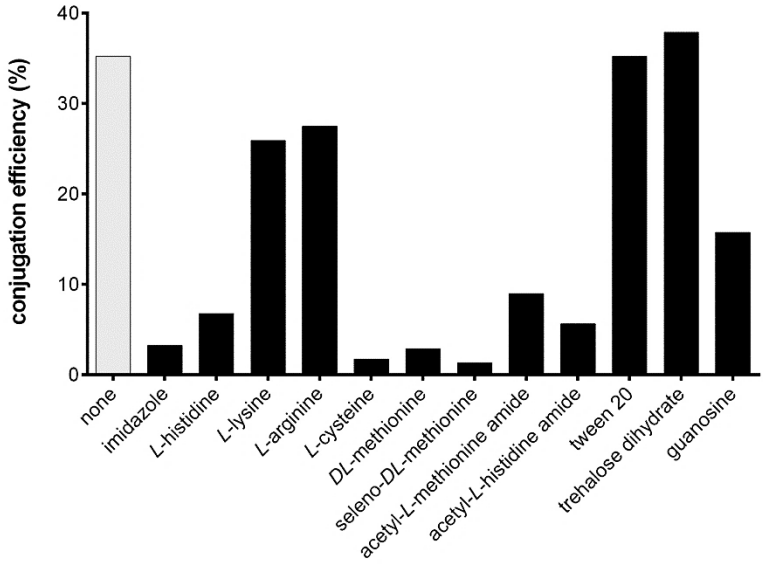

Figure S9. The effect of various additives.

As expected, a decrease of the conjugation efficiency was observed when additives with a high affinity for Cl-*Lx* (**1a**) were added, thus competing for Pt(II) with the coordination sites on the antibody (Fig. S9). *N*-Heterocycle, thiol, and thioether containing additives resulted in the biggest decrease in the conjugation efficiency. This finding indicates that amino acid residues that are present in the antibody and that contain these functional groups (His, Met, and Cys), are favourable for conjugation to an *Lx* semi-final complex. The most important although not unexpected finding was that added *L*-His has a drastic detrimental effect on the conjugation efficiency. Since it is a component of the formulation buffer of Herceptin®, we considered its removal as the next logical and promising step to further increase the conjugation efficiency (this will be described in section 3.11.).

A minor decrease in efficiency was observed when Lys and Arg were used as additives; however, these amino acids are not expected to form stable complexes with Pt(II). Besides, the observed weaker conjugation inhibition by these two residues is in accordance with our working hypothesis that the preferential binding position of *Lx* on antibodies are His residues.

To get insight into the question if the addition of NaI – the crucial finding of section 3.5.1. – influences the binding site of *Lx* on the antibodies (*i.e.* if the same subset of amino acid residues is addressed by *Lx* depending on the presence of NaI in the conjugation mixture), it was decided to test the crucial amino acid and amino acid derivatives also in the absence of NaI.

Table S12. Screening of various additives without co-addition of NaI.

Entry	Buffer	Buffer concentration (mM)	Buffer pH	Additional salt in the buffer	Additional salt concentration (mM)	Eq. of *Lx* used in the conjugation	Additive	Additive concentration (mM)
167-176	HEPES	20	8.1	none	0	20	see Table S11	30

To be able to compare the conjugation efficiencies obtained with and without NaI in a direct manner, the results were normalized in respect to conjugation efficiencies – 19.8% and 35.2% without and with the addition of NaI, respectively – obtained when no amino acid additive was used. In other words, the conjugation efficiencies without amino acid additives were assigned 100% and the percentages obtained in the presence of these amino acid additives reflected the extent to which these additives inhibited the conjugation.

The results (Fig. S10; also Fig. 3 of the main manuscript) showed that coordination to Arg, Cys, and Lys is not influenced by the addition of NaI, and that their detrimental effect on the conjugation efficiency ratio is similar for conjugations with and without NaI.

More interesting are results of the *N*-heterocycle containing additives (His and imidazole) in which significantly less relative conjugation efficiency was observed when NaI was used compared to the control conjugation. This indicates that the addition of NaI enhances the coordination of *Lx* to His residues of an antibody. Since the opposite effect can be seen for Met (and to a less extent Cys and Arg), it can also be concluded that coordination to Met is suppressed when NaI is used. This is an interesting and important observation since it indicates that addition of NaI steers/facilitates the *Lx*-conjugation to the desired binding sites on an antibody (*i.e.* to His residues), thus improving the selectivity of the *Lx*-binding besides improving the overall binding efficiency. This finding will be described in more detail in section 3.10.

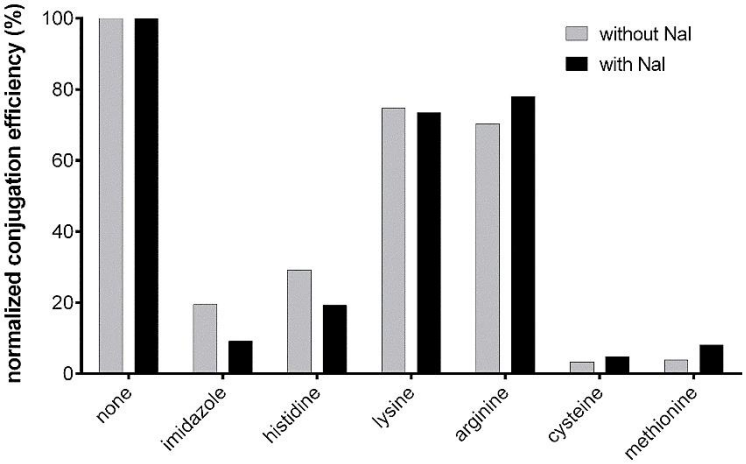

Figure S10. The conjugation efficiency in the presence of amino acid additives, with and without NaI. The results were normalized using control conjugations without amino acid additives. The conjugation efficiency of conjugations without amino acid additives: 19.8% (without NaI) and 35.2% (with NaI).

3.7. Fine-tuning of the Cl-*Lx* (1a) stoichiometry in the conjugation reaction

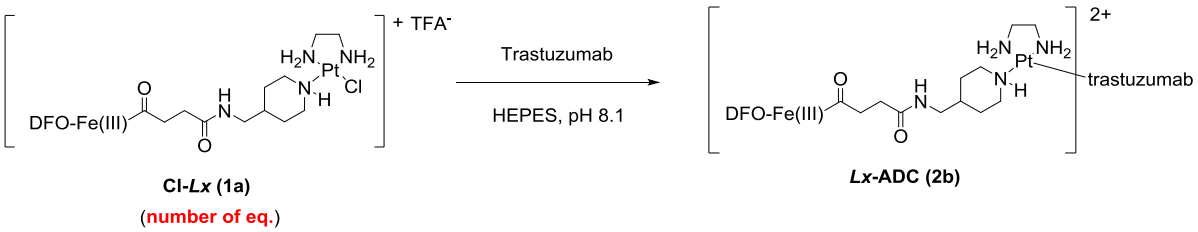

Scheme S8. Fine-tuning of the Cl-*Lx* (**1a**) stoichiometry.

All conjugation reactions in the previous sections were performed with a large excess of 20 eq. of Cl-*Lx* (**1a**), which was necessary to obtain a product with a DAR of 2-3 using the initial conjugation conditions.

After optimization of buffer and the crucial finding on the effect of NaI on the conjugation reaction, the conjugation efficiency was already increased from ~15% to ~**38%**. This means that less equivalents of *Lx* are needed at this stage to produce an ADC with a DAR of 2-3.

To investigate whether a saturation of available His residues was already reached in the previous experiments - an efficiency of 35% using 20 eq. of a payload gives a DAR of ~8 -, it was decided to perform an experiment using less equivalents of Cl-*Lx* (**1a**).

Conjugation procedure: Trastuzumab in its native clinical formulation and Cl-*Lx* (**1a**) (5 eq., 10 eq., and 20 eq.) were incubated in HEPES/NaI (in the concentration range 0-100 mM), pH 8.1 at 47 ^{o}C (Table S13). After the conjugation followed by treatment with a solution of TU, the mixtures were analyzed by SEC to determine the conjugation efficiency (Fig. S11).

Table S13. Fine-tuning of the Cl-*Lx* (**1a**) stoichiometry.

Entries	Buffer	Buffer concentration (mM)	pH buffer	Additional salt in the buffer	Additional salt concentration range (mM)	Eq. of *Lx*
177-182	HEPES	20	8.1	NaI	0-100	5
183-188	HEPES	20	8.1	NaI	0-100	10
189-194	HEPES	20	8.1	NaI	0-100	20

Noteworthy, saturation of all available His present in trastuzumab seems not to occur when 20 eq. of Cl-*Lx* (**1a**) were used since no dramatic increase in the conjugation efficiency was found when less equivalents of Cl-*Lx* (**1a**) are used (Fig. S11). An increase to ~**48%** was observed with 5 eq. Cl-*Lx* (**1a**).

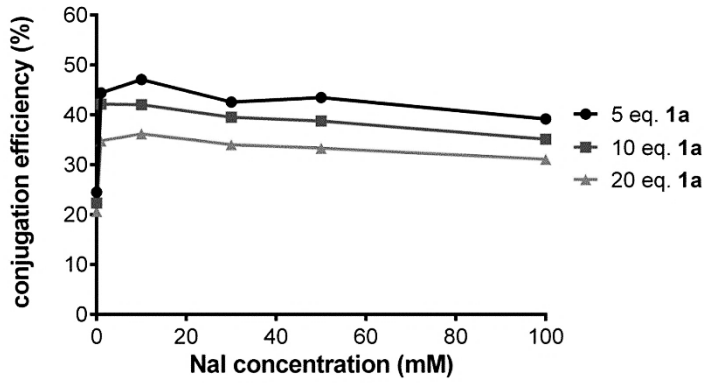

Figure S11. Effect of the Cl-*Lx* (**1a**) stoichiometry on the *Lx*-conjugation efficiency at different concentrations of NaI.

From this point, we started to use 5 eq. of the Cl-*Lx* complex (**1a**) routinely, if not stated otherwise. Using this stoichiometry, not all antibody binding sites that are available for the *Lx*-coordination are saturated and the conjugates that are prepared should have a DAR in the same range as before the start of the optimization, *i.e.* 2-3.

3.8. Screening of the conjugation temperature and time

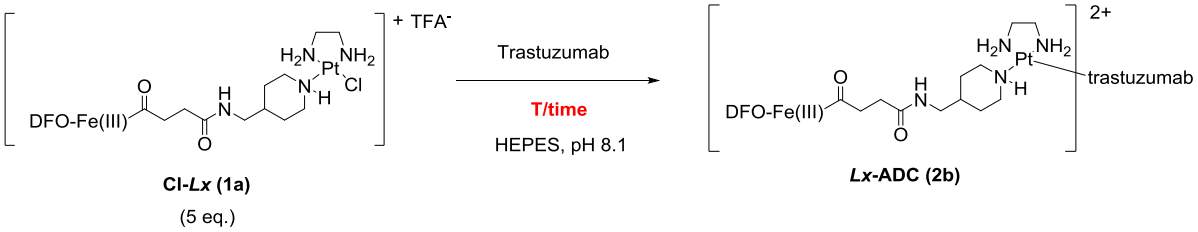

Scheme S9. Screening of the conjugation temperature and time.

Temperature is an important reaction parameter that usually strongly influences the reaction kinetics. However, in the case of mAbs, an increase of temperature may result in decomposition, formation of aggregates or total denaturation of the protein.

In this experiment (Table S14), the effects of reaction temperature on the conjugation efficiency, kinetics, and the protein integrity were investigated. It should be noted that the maximal temperature that an antibody can tolerate needs to be optimized for every protein.

Conjugation procedure: Trastuzumab in its native clinical formulation and Cl-*Lx* (**1a**) (5 eq.) were incubated in HEPES/NaI, pH 8.1 at five different temperatures (Table S14) and samples were taken after 1 h, 2 h, 4 h, 6 h, and 24 h. After the conjugation followed by treatment with a solution of TU, the mixtures were analyzed by SEC to determine the conjugation efficiency (Fig. S12 and Table S15).

Table S14. Conjugation at different temperatures.

Entries	Buffer	Buffer concentration (mM)	Buffer pH	Additional salt in the buffer	Additional salt concentration (mM)	Eq. of *Lx*	Reaction temperature (°C)	Reaction time (h)
195-199	HEPES	20	8.1	NaI	10	5	22	1-24
200-204	HEPES	20	8.1	NaI	10	5	37	1-24
205-209	HEPES	20	8.1	NaI	10	5	47	1-24
210-214	HEPES	20	8.1	NaI	10	5	57	1-24
215-219	HEPES	20	8.1	NaI	10	5	67	1-24

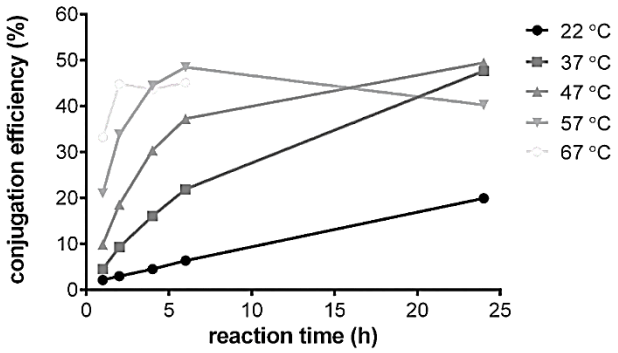

Figure S12. The conjugation efficiency at five different temperatures.

Table S15. Results of the temperature and time screening.

Entries	Conjugation T [oC]	Conjugation time [h]	Conjugation efficiency [%]	Aggregation level [%]
195-199	22 °C	24	20	0.5
200-204	37 °C	24	48	0.9
205-209	47 °C	24	**49**	1.5
210-214	57 °C	24	40	3.1
215-219	67 °C	6[a]	45	22.5[b]

[a] Conjugation reaction discontinued
[b] SEC chromatogram of trastuzumab in Fig. S13

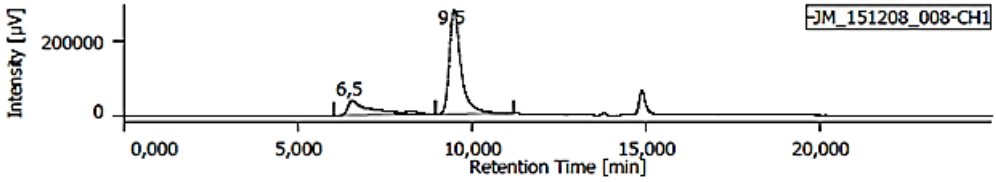

Figure S13. SEC chromatogram (280 nm) of trastuzumab after 6 h conjugation time at 67 °C.

Expectedly, the temperature increase resulted in an increase of the conjugation rate (Fig. S12). However, temperatures higher than 47 °C resulted in increased amounts of antibody aggregation (Table S15 and Fig. S13), clearly showing thermal limits that trastuzumab can tolerate. Therefore, conjugation experiments were continued at 47 °C, a maximally tolerated optimal temperature for trastuzumab (**49%** efficiency after 24 h conjugation time, Table S15) that retains the antibody integrity (all tested mAbs tolerated this temperature, see section 3.12.; however, for temperature sensitive mAbs or for settings where exact and homogeneous temperature control is challenging (*e.g.* in case of a large scale conjugation), the *Lx*-conjugation could be run at a lower temperature). As can be seen from Fig. S12, for conjugation times >24 h conjugations can be performed at 37 °C with a similar efficiency.
Typical conjugation time to achieve a complete *Lx*-conjugation is ~24 h.

3.9. Pre-activation of Cl-*Lx* (1a) by iodide exchange

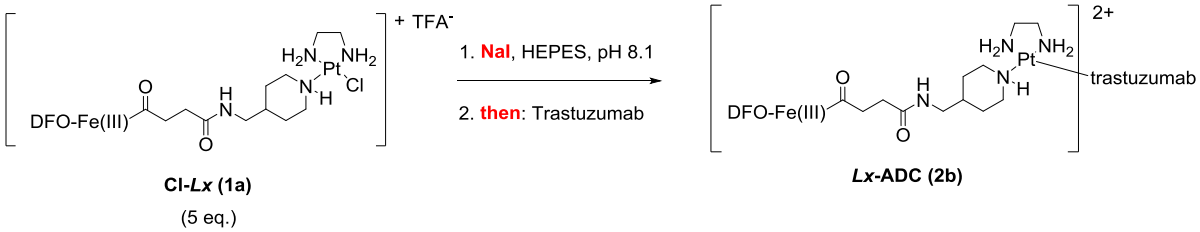

Scheme S10. Pre-activation of Cl-*Lx* (**1a**) before the *Lx*-conjugation.

It was anticipated that a pre-treatment of Cl-*Lx* (**1a**) with NaI can result in an improved conjugation rate. Since our hypothesis for the improved conjugation efficiency upon addition of NaI to the conjugation mixture was the formation of a more reactive intermediate I-*Lx* (**1c**), it could be advantageous to pre-activate Cl-*Lx* (**1a**), thus forming I-*Lx* (**1c**), before the addition of trastuzumab to the conjugation mixture.

Conjugation procedure: Cl-*Lx* (**1a**) (5 eq.) was first pre-activated with NaI using three different pre-activation methods **A**-**C** (Table S16; method **D** was a control experiment without NaI addition in the pre-activation step), differing in the pre-activation time and temperature. Then, after addition of trastuzumab in its native clinical formulation to the pre-activated mixture, the mixtures were incubated in HEPES/NaI, pH

8.1 at 47 °C and samples were taken after 1 h, 2 h, 4 h, 6 h, and 24 h. After the conjugation followed by treatment with a solution of TU, the mixtures were analyzed by SEC to determine the conjugation efficiency (Fig. S14).

Table S16. Conjugation with pre-activation of Cl-*Lx* (**1a**).

Entries	Buffer	Buffer concentration (mM)	Buffer pH	Additional salt in the buffer	Additional salt concentration (mM)	Eq. of *Lx*	Reaction temperature (°C)	Reaction time (h)	Cl-*Lx* pre-activation method
220-224	HEPES	20	8.1	NaI	10	5	47	1-24	**none**
225-229	HEPES	20	8.1	NaI	10	5	47	1-24	**A**
230-234	HEPES	20	8.1	NaI	10	5	47	1-24	**B**
235-239	HEPES	20	8.1	NaI	10	5	47	1-24	**C**
240-244	HEPES	20	8.1	NaI	10	5	47	1-24	**D**

- **method A**: incubation of Cl-*Lx* (**1a**) in the HEPES buffer with NaI (50 eq.) at 47 °C for 2 h, followed by the addition of trastuzumab (entries 225-229)
- **method B**: incubation of Cl-*Lx* (**1a**) in the HEPES buffer with NaI (50 eq.) at 47 °C for 24 h, followed by the addition of trastuzumab (entries 230-234)
- **method C**: incubation of Cl-*Lx* (**1a**) in the HEPES buffer with NaI (50 eq.) at 37 °C for 24 h, followed by the addition of trastuzumab (entries 235-239)
- **method D (control)**: incubation of Cl-*Lx* (**1a**) in the HEPES buffer without NaI at 47 °C for 24 h, followed by the addition of trastuzumab (entries 240-244)

Control conjugations were performed without the pre-activation step (entries 220-224) to compare with the effect of pre-activation with NaI (**methods A**, **B**, and **C**); incubation in the absence of NaI (**method D**) was used as a control for stability of Cl-*Lx* (**1a**) at 47 °C in the HEPES buffer.

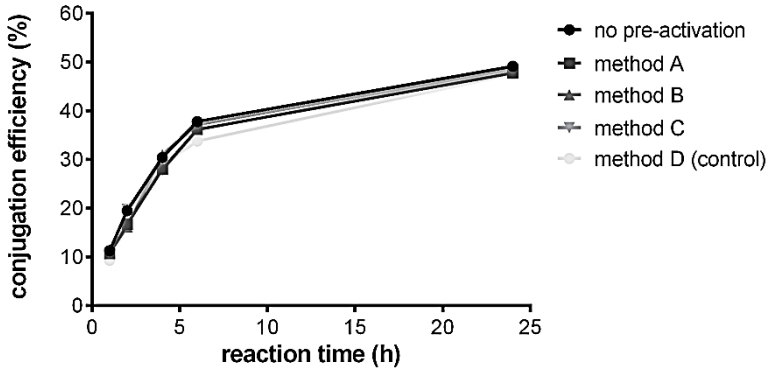

Figure S14. The conjugation efficiency using different pre-activation methods of Cl-*Lx* (**1a**).

Results from this experiment (Fig. S14) indicated that a pre-treatment of Cl-*Lx* (**1a**) did not result in a better conjugation efficiency. Even at shorter conjugation times no significant increase in efficiency was observed. The conclusion from this experiment can be that the formation of an iodido Pt(II) complex such as I-*Lx* (**1c**) from a chlorido Pt(II) complex such as Cl-*Lx* (**1a**) – in case NaI is present – occurs very rapidly during the conjugation. Therefore, the beneficial effect on the conjugation efficiency using a pre-formed iodido Pt(II) complex **1c** is negligible. To further support the hypothesis that iodido Pt(II) complex **1c** is formed as an intermediate which is very reactive towards certain binding sites on the antibody surface, this I-*Lx*

intermediate **1c** was synthesized, isolated, and used in the conjugation reaction instead of the thus far standardly used Cl-*Lx* semi-final complex **1a** (will be described in section 3.13.).

3.10. The effect of the TU quenching step on the conjugation efficiency

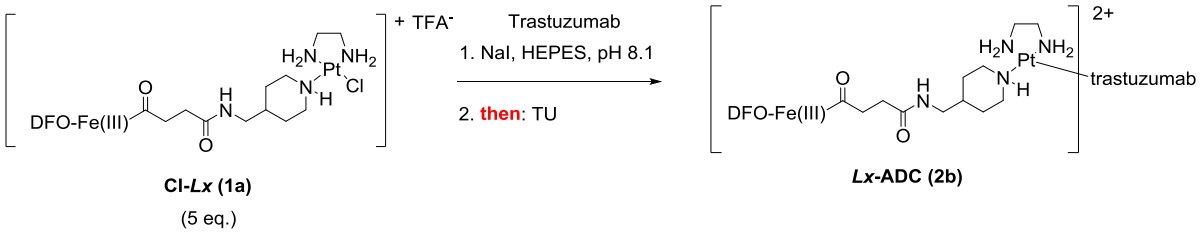

Scheme S11. The effect of the TU quenching/washing step.

The thiourea (TU) quenching/washing step is a work-up step that provides stable, well-defined, and reproducible *Lx*-conjugates by removing the weakly bound *Lx*-complexes via formation of strong TU-*Lx* complexes.[8]

After the discovery that NaI (and NaBr to a lesser extent) considerably improved the conjugation efficiency (as discussed in section 3.5.1.) and furthermore the method became more selective towards the desired His targeting (as it was discussed in section 3.6.), it was decided to test the efficiency of the TU quenching step again (Table S17).

We expected the effect of the TU quenching step to decline, and the difference in the conjugation efficiency before and after the TU quenching step can indicate selective His binding.

Conjugation procedure: Trastuzumab in its native clinical formulation buffer and Cl-*Lx* **1a** (5 eq.) were incubated in HEPES/NaI (absent or present during the conjugation), pH 8.1 at 47 ^{o}C, and samples were taken after 1 h, 2 h, 4 h, 6 h, and 24 h. After the conjugation, the mixture was either treated or not treated with a solution of TU (Table S17). The mixtures were analyzed by SEC to determine the conjugation efficiency (Fig. S15).

Table S17. Experiment on the effect of the TU quenching/washing step.

Entries	Buffer	Buffer concentration (mM)	Buffer pH	Additional salt in the buffer	Additional salt concentration (mM)	Eq. of *Lx*	Reaction temperature (^{o}C)	Reaction time (h)	TU quenching step after the conjugation
245-249	HEPES	20	8.1	none	0	5	47	1-24	no
250-254	HEPES	20	8.1	none	10	5	47	1-24	yes
255-259	HEPES	20	8.1	NaI	10	5	47	1-24	no
260-264	HEPES	20	8.1	NaI	10	5	47	1-24	yes

In the absence of NaI (Fig. S15, gray lines), the difference between the efficiency before and after the TU quenching step was significant for reaction times until 6 h, which indicates that at short reaction times a significant amount of weakly bound *Lx*-complexes were formed. However, since the binding of Pt(II)

complexes to Met is a kinetic effect and these complexes are not thermodynamically stable, the difference in the conjugation efficiencies becomes hardly detectable at prolonged reaction times (24 h).

In contrast, in the presence of NaI (Fig. S15, black lines), the observed efficiencies are not only higher, but the effect of the TU quenching step on the conjugation efficiencies became hardly detectable for all conjugation times measured.

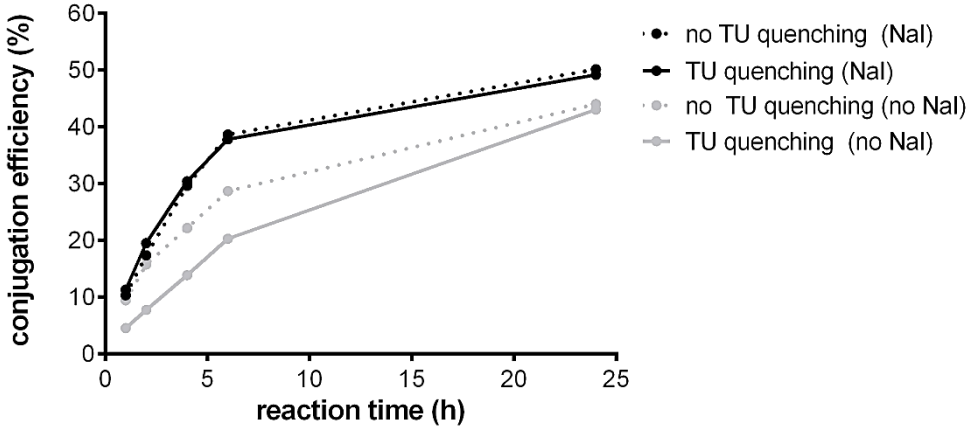

Figure S15. The effect of the TU quenching step in the presence (black lines) or absence (gray lines) of NaI.

As next, the effect of temperature and reaction time on the stability (*i.e.* aggregate formation) of the mAb during the TU quenching step was investigated. To this end, we prepared the ADC trastuzumab-*Lx*-DFO-Fe(III) (**2b**) by reaction of trastuzumab with I-*Lx* (**1c**). The non-purified conjugate mixture was divided into 17 equal parts and treated (except for one control sample) with an aqueous solution of TU (10 mM final concentration in the conjugation mixture) at four different temperatures (4 ^{o}C, 22 ^{o}C, 37 ^{o}C, and 47 ^{o}C). The quenched reaction mixtures were purified after 5 min., 15 min., 30 min., and 24 h reaction time and subsequently analyzed (Fig. S16).

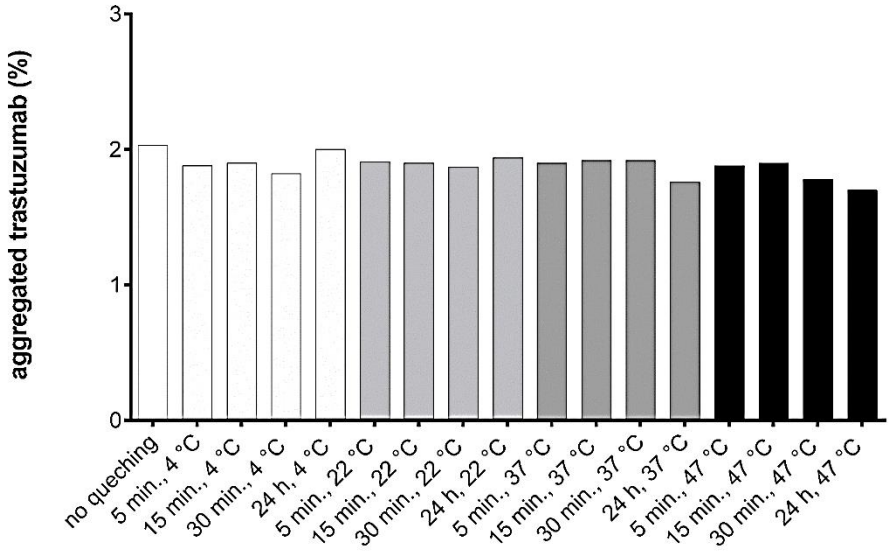

Figure S16. Aggregate formation during the TU quenching step.

After the TU quenching step was performed at four temperatures and four reaction times, it became clear that this process is rapid (finished after 5 min. even at 4 ^{o}C) and can also be performed at 47 ^{o}C, *i.e.* the

conjugation temperature, without affecting the antibody integrity (similar aggregation levels were observed; Fig. S16).

Although the TU quenching step might seem obsolete if iodide is used as an additive, it still offers important advantages, especially for a large-scale manufacturing. Namely, this process step ensures a rapid and quantitative termination of the *Lx*-conjugation reaction by quenching the reactive semi-final precursor complex **1**, thus forming a non-conjugatable and easily removable payload-containing TU-adduct (see section 7.3.4.).

3.11. The buffer exchange from the Herceptin® formulation buffer

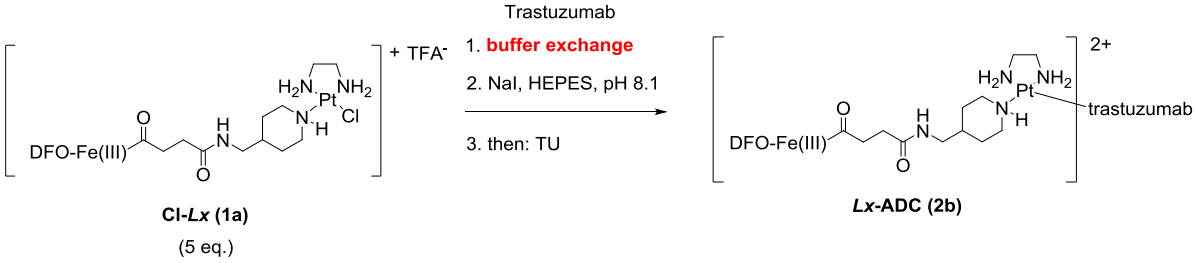

Scheme S12. Buffer exchange of the Herceptin® formulation buffer.

As observed in section 3.6., presence of certain thiol, thioether or amine containing groups (*e.g.* Cys, Met, His, *etc*.) in the conjugation mixture can greatly decrease the conjugation efficiency of the reaction of Pt(II) complexes with trastuzumab. Compounds containing such reactive groups are able to capture the *Lx* semi-final complexes leading to their non-productive consumption. Antibodies are usually stored in a formulation buffer and it is important to make sure that such critical excipients are removed before the conjugation reaction will take place.

To this end, we designed an experiment (Table S18) to investigate the influence of buffer exchange of trastuzumab (Herceptin®) from its pharmacy formulation buffer into a buffer which is better suited to be used in the *Lx*-conjugation.

Conjugation procedure: Trastuzumab, after exchange of its native Herceptin® clinical formulation buffer (Table S19), and Cl-*Lx* **1a** (5 eq.) were incubated in HEPES/NaI, pH 8.1 at 47 °C. After the conjugation followed by treatment with a solution of TU, the mixtures were analyzed by SEC to determine the conjugation efficiency (Fig. S17).

Table S18. Experiment on the buffer exchange of Herceptin®.

Entry	Buffer	Buffer concentration (mM)	Buffer pH	Additional salt in the buffer	Additional salt concentration (mM)	Eq. of *Lx*	Reaction temperature (°C)	Reaction time (h)	Formulation buffer of the antibody
265-274	HEPES	20	8.1	NaI	10	5	47	24	see Table S19

The formulation buffer of trastuzumab (Herceptin®) consists of *L*-His × HCl, *L*-His, TWEEN® 20, and trehalose dihydrate (Table S19, pharmacy buffer A). Since the His residues are expected to be the most

likely binding sites for Pt(II) binding in native mAbs, we expected the conjugation efficacy to increase after buffer exchange of the antibody into a non-His containing buffer. For this screening experiment, we have chosen 10 formulation buffers (Table S19): 9 alternative formulation buffers and 1 (pharmacy buffer A having the exact composition of the Herceptin® formulation buffer) used as a control. First, we prepared two buffers which were analogous to the native pharmacy buffer but lacked *L*-His (pharmacy buffer B) or two main components of the Herceptin® formulation buffer: *L*-His and the surfactant TWEEN® 20 (pharmacy buffer C). Moreover, we selected several buffers which are commonly used for conjugation of small molecules to proteins (saline, PBS). Diluted saline (0.45% NaCl) was used to determine the effect of the NaCl concentration.

Since the conjugations were performed in the HEPES buffer (and the tricine buffer before the results of the current optimization were obtained), a direct buffer exchange of the protein into the HEPES buffer (or tricine) was also considered. And since a significant increase of the conjugation efficiency was observed with NaI as an additive, also buffer exchange of the protein into a 0.9% NaI solution was attempted.

Table S19. Buffers used for the buffer exchange of Herceptin®.

Solution used for the buffer exchange	Contents per liter of such a solution
pharmacy buffer A	495 mg *L*-His × HCl; 320 mg *L*-His; 20 g *α,α*-trehalose × 2 H_2O; 90 mg TWEEN® 20
pharmacy buffer B	20 g *α,α*-trehalose × 2 H_2O; 90 mg TWEEN® 20
pharmacy buffer C	20 g *α,α*-trehalose × 2 H_2O
saline (0.9% NaCl)	9.0 g NaCl
0.45% NaCl	4.5 g NaCl
0.9% NaI	9.0 g NaI
phosphate buffer saline (PBS)	8.2 g NaCl; 1.9 g Na_2HPO_4.× 2 H_2O; 0.3 g NaH_2PO_4 × 2 H_2O (pH 7.4)
10 mM HEPES (pH 8.1)	2.4 g HEPES (set pH to 8.1)
20 mM HEPES (pH 8.1)	4.8 g HEPES (set pH to 8.1)
20 mM tricine (pH 8.1)	3.6 g tricine (set pH to 8.1)

Fig. S17 clearly shows the effect of the removal of *L*-His from the antibody formulation buffer prior to conjugation. All buffers without *L*-His showed similar efficiencies of ~80%, whereas the standard formulation buffer which had been used in all conjugations thus far now only reached ~45% after 24 h conjugation time. Data from the conjugation reaction after the buffer exchange of trastuzumab in 0.9% NaI indicated a significantly higher antibody aggregation peak compared to the other buffers tested. The most likely explanation for this is the instability of trastuzumab in this buffer, which also resulted in a slightly decreased conjugation efficiency.

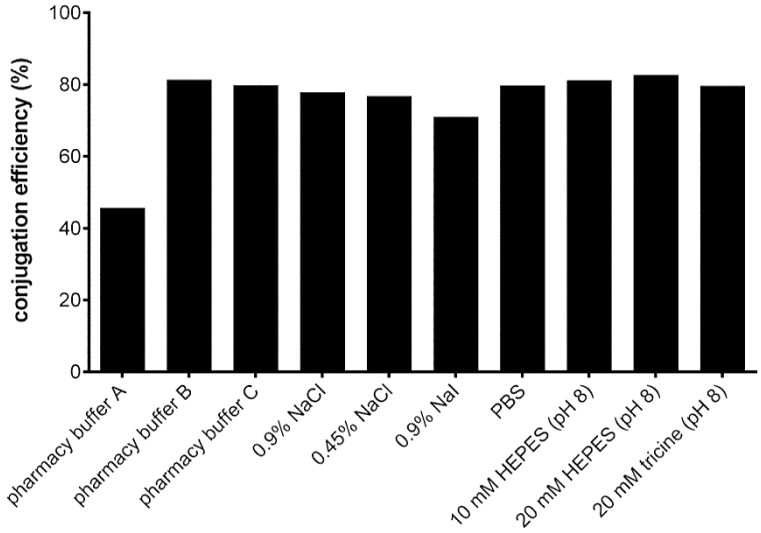

Figure S17. Conjugation efficiency after the buffer exchange of Herceptin® (24 h reaction time).

In order to determine if not only the plateau value of ~80% but also the rate of the conjugation was improved in non-His containing buffers, an experiment was performed (Table S20) where the conjugation of Cl-*Lx* (**1a**) to trastuzumab in the pharmacy buffer A, in 10 mM HEPES, and in PBS was compared with increasing reaction times.

Table S20: The kinetic experiment after the buffer exchange of Herceptin®.

Entries	Buffer	Buffer concentration (mM)	Buffer pH	Additional salt in the buffer	Additional salt concentration (mM)	Eq. *Lx*	Reaction temperature (°C)	Reaction time (h)	Antibody buffer
275-279	HEPES	20	8.1	NaI	10	5	47	1-24	pharmacy buffer A
280-284	HEPES	20	8.1	NaI	10	5	47	1-24	10 mM HEPES
285-289	HEPES	20	8.1	NaI	10	5	47	1-24	PBS

Results are displayed in Fig. S18. When the native pharmacy buffer A was used, the increase in efficiency was almost linear during the first 6 h. However, between 6 h and 24 h, only a minor additional increase (from ~35% to ~45%) of the conjugation efficiency was observed, indicating that the major part of the semi-final complex **1a** has reacted with His in solution or with the His residues of the antibody in the first ~6 h.

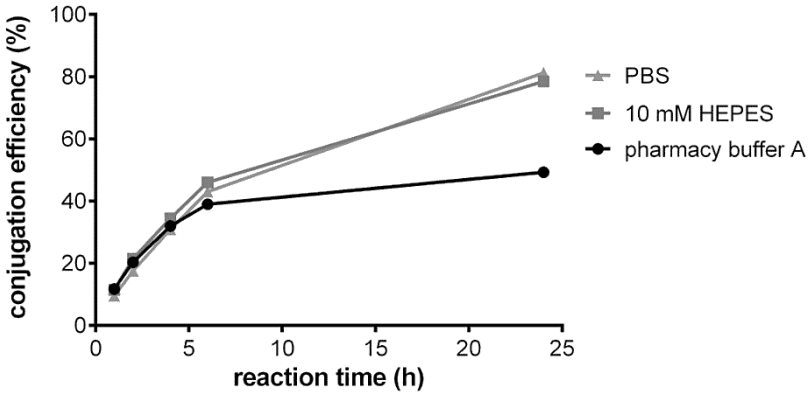

Figure S18. Kinetics of the conjugation efficiency after the Herceptin® buffer exchange.

Instead, when 10 mM HEPES or PBS were used, we observed similar conjugation efficiencies compared to the pharmacy buffer A during the first 6 h of the conjugation. Thus, the buffer exchange did not increase the rate of the conjugation. However, because there is no competition with the free *L*-His in solution, there is still reactive semi-final complex present in the conjugation mixture, resulting in a higher plateau value of ~80% after 24 h.

All non-His containing buffers that were tested showed similar results, which means that the conjugation reaction can be performed without loss of efficiency in a broad range of conjugation buffers that do not contain *Lx*-capturing components. Consequently, it was decided to buffer exchange the protein to phosphate buffered saline (PBS) solution as a standard buffer for the *Lx*-conjugations.

3.12. Conjugation with various mAbs

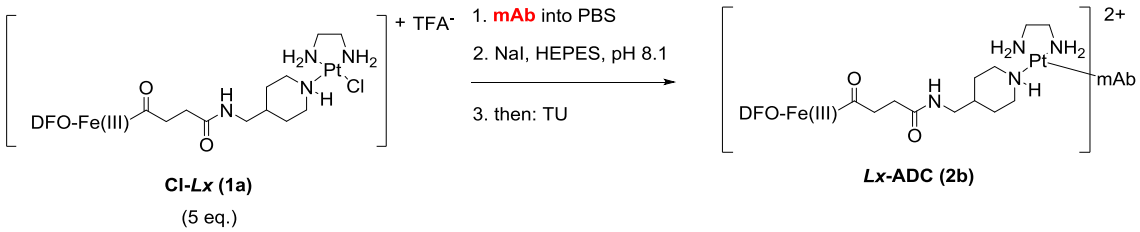

Scheme S13. Conjugation with various mAbs.

Our working hypothesis, supported by several indirect experimental evidences and literature, is that the *Lx*-conjugation targets His residues of native antibodies forming thermodynamically stable conjugates. Fortunately, by nature most of the His residues present in mAbs are located in the non-variable parts, mainly in the Fc region, and not in the variable antigen recognition sites.

Therefore, since the most prominent binding sites are the same in all mAbs, other mAbs should show *Lx*-conjugation efficiencies comparable to trastuzumab. To confirm this, we tested the conjugation of Cl-*Lx* (**1a**) with several available antibodies that were buffer exchanged into PBS (section 3.11.) and reconstituted to 21 mg/mL before use in the *Lx*-conjugation.

Performed experiments are summarized in Table S21.

Conjugation procedure: A mAb (Table S22), after exchange of its native clinical formulation buffer into PBS, and Cl-*Lx* (**1a**) (5 eq.) were incubated in HEPES/NaI, pH 8.1 at 47 °C and samples were taken after 2 h

and 24 h. After the conjugation followed by treatment with a solution of TU, the mixtures were analyzed by SEC to determine the conjugation efficiency (Fig. S19).

Table S21. Conjugation conditions used for various antibodies.

Entries	Buffer	Buffer concentration (mM)	Buffer pH	Additional salt in the buffer	Additional salt concentration (mM)	Eq. *Lx*	Reaction temperature (°C)	Reaction time (h)	Antibody buffer	Antibody
290-296	HEPES	20	8.1	NaI	10	5	47	2	PBS	see Table S22
297-303	HEPES	20	8.1	NaI	10	5	47	24	PBS	see Table S22

Table S22. Tested mAbs.

Antibody	Trade name	Target
Trastuzumab	Herceptin®	HER2/neu
Cetuximab	Erbitux®	EGFR
Rituximab	Rituxan,® MabThera,® and Zytux®	CD20
Ofatumumab	Arzerra®	CD20
Obinutuzumab	Gazyvaro®	CD20

Trastuzumab, cetuximab, rituximab, ofatumumab, and obinutuzumab are FDA approved mAbs currently used in the therapy for treatment of various diseases. Not all antibodies are suitable for use in ADCs; they were included in this experiment to test the general applicability of the thus far optimized *Lx*-conjugation method.

The five tested antibodies showed results comparable to trastuzumab and conjugation efficiencies of 74-78% after 24 h conjugation time (Fig. S19).

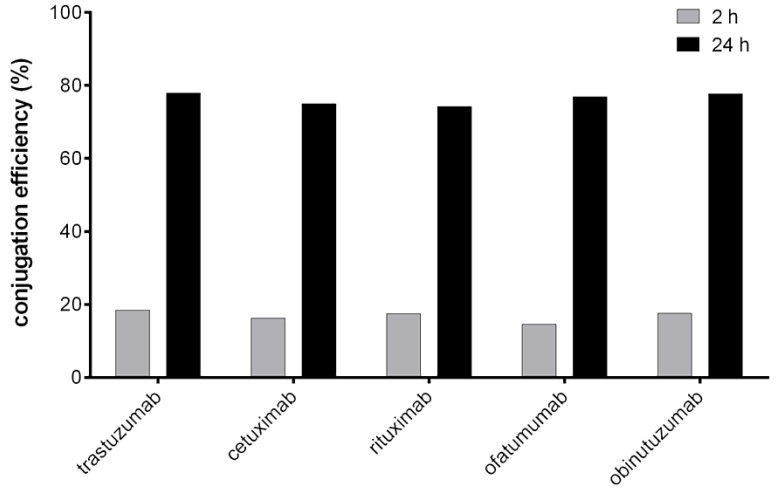

Figure S19. Conjugation efficiency with various antibodies.

Since these antibodies contain a similar number of His (and a similar distribution over the antibody surface), these results were expected and they confirmed the generality of the *Lx*-conjugation and our working hypothesis of the His targeting.

3.13. Conjugation of semi-final complexes bearing different halido leaving groups

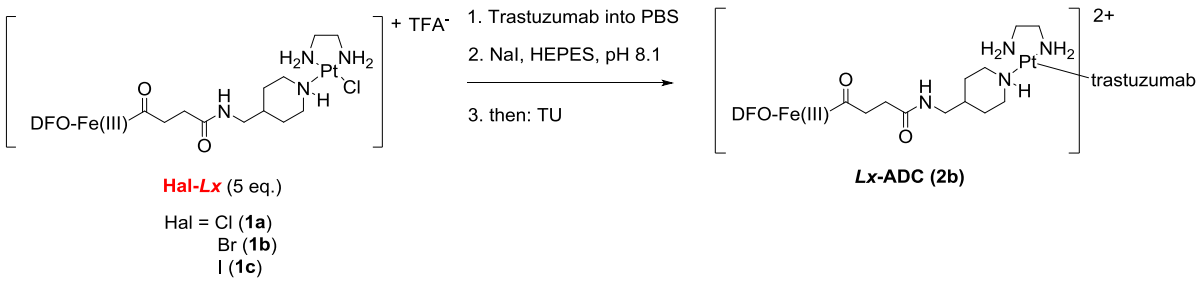

Scheme S14. Conjugation of semi-final complexes Hal-*Lx* (**1a-c**).

The most striking finding (described in section 3.5.1.) of the current optimization was a significant increase in the conjugation efficiency in the presence of an iodide source, *e.g.* upon addition of NaI to the conjugation mixture. It is assumed that the observed effect of an iodide salt on the conjugation efficiency is not the result of an interaction of the iodide anion with the protein, but that it is most likely caused by a rapid exchange of the chloride leaving group of Cl-*Lx* (**1a**) by the iodide ligand. The present experiments clearly indicated that such an iodido Pt(II) complex must have been formed as a more reactive intermediate during the conjugation of Cl-*Lx* (**1a**) to an antibody – an observation which was unexpected based on literature present at the time the described experiments were conducted, describing a diiodido Pt(II) complex as being less reactive towards a model nucleotide (*i.e.* an *N*-nucleophile) compared to its dichlorido analog.[9]

To learn more about the surprising reactivity of the present iodido Pt(II) complexes, model complexes I-*Lx* (**1c**) and Br-*Lx* (**1b**) were synthesized (Scheme S15) which differ from the complex Cl-*Lx* (**1a**) only in their leaving halido group on the Pt(II) center. We also synthesized the unreactive TU-*Lx*-DFO-Fe(III) complex TU-*Lx* (**1e**) to investigate if this complex – which is a product of the TU quenching step with excessive Cl-*Lx* (**1a**) in the conjugation mixture (see section 7.3.4.) – remains inert in the presence of an excess of NaI.

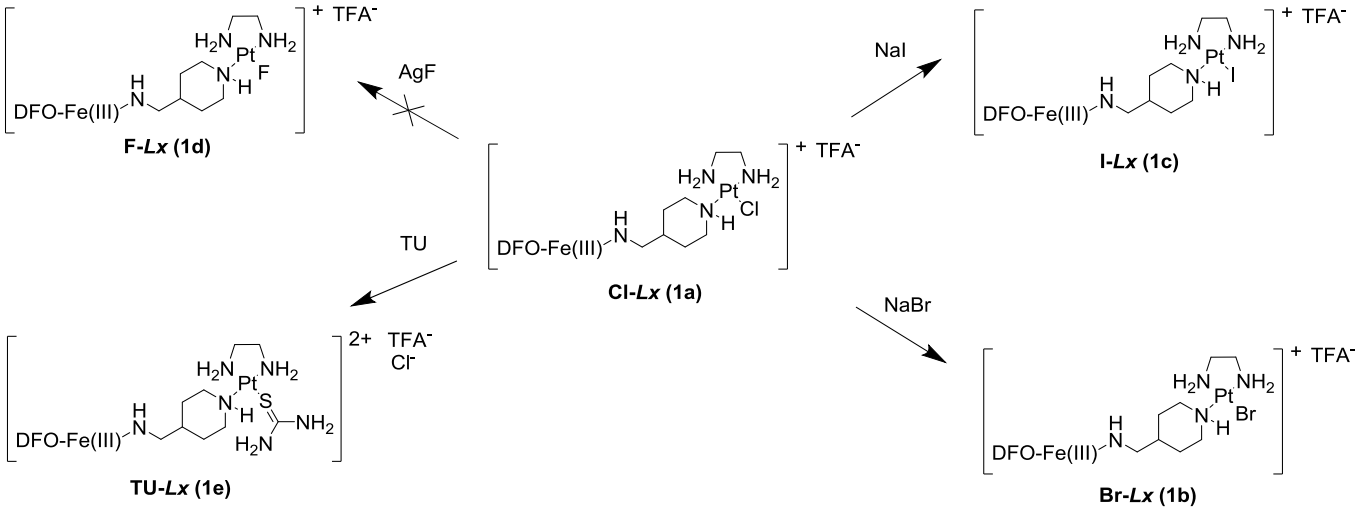

Scheme S15. Synthesis of semi-final complexes bearing various halido leaving groups (**1a-d**) or TU (**1e**).

Addition of NaI (6.4 eq.) to Cl-*Lx* (**1a**) resulted in an almost immediate conversion to I-*Lx* (**1c**) based on C18 Alltima HPLC analysis, and the pure product was obtained after preparative HPLC (96% at 430 nm). The same procedure was used for the synthesis of Br-*Lx* (**1b**) using 10 eq. of NaBr. Further, TU-*Lx* (**1e**) was synthesized using 1 eq. of TU. Here, an almost complete conversion was observed (C18 Alltima HPLC) after 1 h, and the product **1e** (95% purity at 430 nm) was directly used in the conjugation reaction without further purification.

Similar to the synthesis of the Br-*Lx* (**1b**) and I-*Lx* (**1c**) complexes, synthesis of the corresponding F-*Lx*-DFO-Fe(III) complex F-*Lx* (**1d**) was attempted using AgF. This soluble silver salt was supposed to facilitate the product formation by abstraction of the chlorido ligand from the complex **1a** by Ag^+ while offering F^- as a ligand. However, the product was too hydrolytically unstable – an observation fully in line with the hydrolytical stability tendency (**1c** > **1b** > **1a** > **1d**) among the homologous halido complexes – and only the hydrolyzed product could be obtained after preparative HPLC. This indicated that the fluoride complex **1d** was very unstable and therefore of no practical use for the *Lx*-conjugation reactions.

Table S23 shows all conjugations performed with the *Lx*-complexes **1a**, **1c**, and **1e**. Optimized conditions from previous experiments were used and trastuzumab was buffer exchanged into PBS before use. The conjugations were performed with and without an excess of NaI to determine whether the leaving group present in the Pt(II) complex can indeed be replaced by the iodido leaving group.

Table S23. Conjugation conditions with various leaving groups.

Entries	Buffer	Buffer concentration (mM)	Buffer pH	Additional salt in the buffer	Additional salt concentration (mM)	Eq. *Lx*	Reaction temperature (°C)	Reaction time (h)	Antibody buffer	Leaving group on the *Lx* complex
304-308	HEPES	20	8.1	none	0	5	47	1-24	PBS	Cl
309-313	HEPES	20	8.1	none	0	5	47	1-24	PBS	I
314-318	HEPES	20	8.1	none	0	5	47	1-24	PBS	TU
319-323	HEPES	20	8.1	NaI	10	5	47	1-24	PBS	Cl
324-328	HEPES	20	8.1	NaI	10	5	47	1-24	PBS	I
329-333	HEPES	20	8.1	NaI	10	5	47	1-24	PBS	TU

Results are displayed in Fig. S20 and Fig. S21. The TU-*Lx* complex **1e** (Table S23; entries 314-318 and 329-333) showed almost no conjugation and the residual conjugation observed was most likely derived from the parent Cl-*Lx* complex **1a** which was still present in small quantities in TU-*Lx* (**1e**).

Since there is no difference in the conjugation efficiencies of complexes **1a** (Table S23; entries 319-323) and **1c** (Table S23; entries 324-328) in the presence of 10 mM NaI (Fig. S20; also Fig. 5B of the main part of the manuscript (the TU-*Lx* curve is omitted there)) even after 1 h conjugation time, the chlorido leaving ligand should have been replaced by the iodido leaving group very rapidly and efficiently.

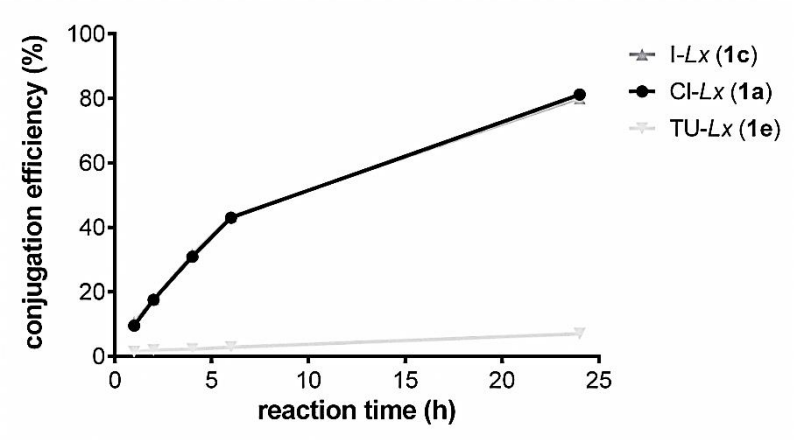

Figure S20. The conjugation efficiency of complexes bearing Cl, I, and TU as ligands on Pt(II) in the presence of NaI.

Fig. S21 proves that the iodido complex **1c** (Table S23; entries 309-313) is indeed more reactive compared to the chlorido complex **1a** (Table S23; entries 304-308). However, a difference in the efficiency of the conjugation of complex **1c** in the presence of excess of NaI (80%) and in the absence of added NaI (55%) was observed.

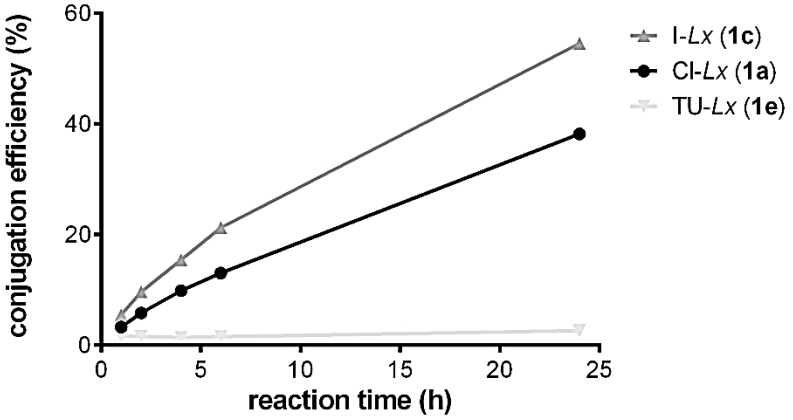

Figure S21. The conjugation efficiency of complexes bearing Cl, I, and TU as ligands on Pt(II) in the absence of NaI.

In order to find an explanation for the reduced reactivity of the I-*Lx* complex **1c** in the absence of an excess of NaI in the conjugation mixture, an additional experiment was performed to determine which Pt(II) species are present during the conjugation reaction.

After the conjugation reaction, trastuzumab was removed from the reaction mixture by spin filtration, after which the filtrate fraction was injected on a C18 Alltima HPLC column (Fig. S22). The Fe(III)-DFO group, which is present in all possible reactive platinum species, was monitored at 430 nm to determine which leaving groups on Pt(II) were present during the conjugation.

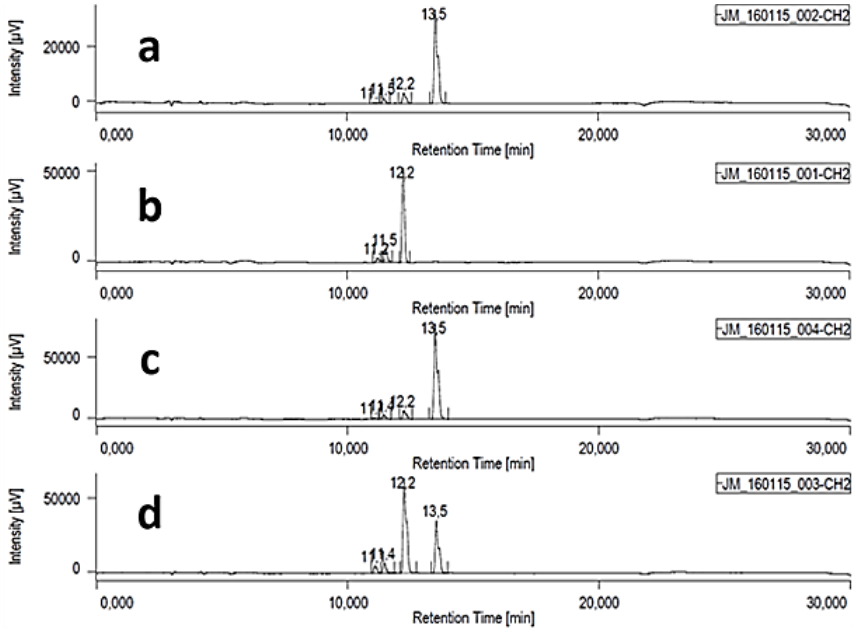

Figure S22. C18 Alltima HPLC chromatograms (at 430 nm) of the filtrates of the conjugation mixtures after removal of the antibody: (**a**) Cl-*Lx* complex **1a** with excess of NaI; (**b**) Cl-*Lx* complex **1a** in the absence of NaI; (**c**) I-*Lx* complex **1c** with excess of NaI; (**d**) I-*Lx* complex **1c** in the absence of NaI.

Fig. S22a shows the HPLC chromatogram of the filtrate of the conjugation mixture of the complex Cl-*Lx* (**1a**) performed in the presence of additional NaI (Table S23; entries 319-323). The main peak at t_R = 13.5 min. corresponds to the I-*Lx* complex **1c**. This, together with the almost completely disappeared peak of Cl-*Lx* (**1a**) (t_R = 12.2 min.), proves the anticipated halide ligand exchange during the conjugation reaction.

Fig. S22b shows the HPLC chromatogram of the filtrate of the conjugation mixture of the complex Cl-*Lx* (**1a**) performed in the absence of additional NaI (Table S23; entries 304-308). Because there is no iodide present, the chlorido leaving group on *Lx* cannot be replaced. Therefore, the main complex present in the conjugation mixture is the Cl-*Lx* starting material **1a** along with presumably its hydrolysis product (t_R = 11.5 min.).

Fig. S22c shows the HPLC chromatogram of the filtrate of the conjugation mixture of the complex I-*Lx* (**1c**) performed in the presence of additional NaI (Table S23; entries 324-328). This chromatogram is comparable with that of Fig. S22a (Cl-*Lx* (**1a**)/NaI). Presence of the same reactive species explains the similar efficiency in the previous conjugation experiment (Fig. S20).

Finally, Fig. S22d shows the HPLC chromatogram of the filtrate of the conjugation mixture of the I-*Lx* complex **1c** performed in the absence of additional NaI (Table S23; entries 309-313). This result shows formation of the less reactive Cl-*Lx* complex **1a**, which explains the lower efficiency observed in Fig. S21 compared to Fig. S20.

We concluded from these results that, although the reactive I-*Lx* complex **1c** was formed very rapidly when the Cl-*Lx* complex **1a** was used with an excess of NaI, formation of the less reactive Cl-*Lx* complex **1a** was also possible when the I-*Lx* complex **1c** was used in combination with an excess of NaCl. Thus, the halide exchange is reversible. Since NaCl was present in a large excess deriving from the PBS conjugation buffer, we observed a lower conjugation efficiency, even when the iodido complex I-*Lx* **1c** was used.

To further prove this hypothesis, conjugation experiments where repeated after buffer exchange of trastuzumab into the HEPES buffer instead of PBS (Table S24). The HEPES buffer does not contain NaCl,

thus the formation of the less reactive Cl-*Lx* species **1a** cannot take place when the more reactive I-*Lx* complex **1c** is used.

Table S24. Conjugation conditions with three different halido leaving ligands on *Lx* in the HEPES buffer (conjugation without NaCl or NaI).

Entries	Buffer	Buffer concentration (mM)	Buffer pH	Additional salt in the buffer	Concentration additional salt (mM)	Eq. *Lx*	Reaction temperature (°C)	Reaction time (h)	Antibody buffer	Leaving group on the *Lx* complex
334-338	HEPES	20	8.1	none	0	5	47	1-24	10 mM HEPES	Cl
339-343	HEPES	20	8.1	none	0	5	47	1-24	10 mM HEPES	Br
344-348	HEPES	20	8.1	none	0	5	47	1-24	10 mM HEPES	I

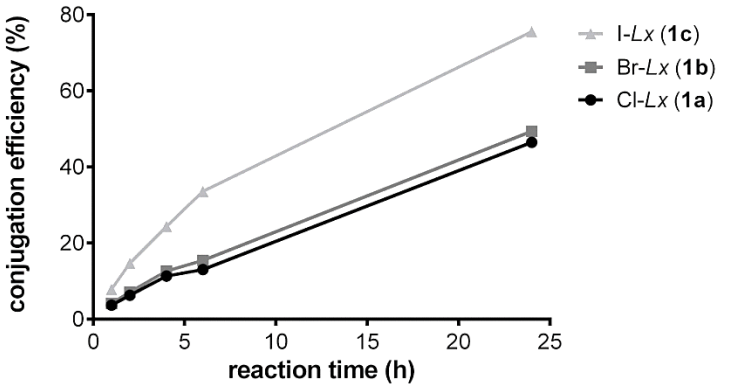

Figure S23. Conjugation efficiency with three different halido leaving groups on *Lx* in the HEPES buffer (no additional salt was added).

Indeed, the I-*Lx* complex **1c** showed the improved reactivity towards trastuzumab compared to the Cl-*Lx* complex **1a** (Fig. S23). The obtained conjugation efficiency (76%) was slightly lower compared to the efficiency obtained in PBS and using an excess of NaI (80%; Fig. S20). Additionally, the conjugation efficiency for the Br-*Lx* complex **1b** was expected to be higher than the efficiency for the Cl-*Lx* complex **1a** and to be somewhere between the efficiencies obtained for the complexes **1a** and **1c**, as described in the experiments using sodium salt additives (section 3.5.1.). In reality, the efficiency obtained using complex Br-*Lx* **1b** (49%) was almost the same as obtained for the Cl-*Lx* complex **1a** (47%).

To search for an explanation of these results, the filtrates of the conjugation mixtures obtained after removal of trastuzumab were analyzed using the C18 Alltima HPLC (Fig. S23). These analyses explain the higher efficiency obtained for the *Lx*-conjugation reactions when additional salt was added (Fig. S21 compared to Fig. S20). Fig. S24a and Fig. S24b show clearly that when the Cl-*Lx* complex **1a** or Br-*Lx* complex **1b** (t_R = 12.0 min. and t_R = 12.4 min., respectively) were used without additives, the complexes appeared to be hydrolyzed considerably already after 1 h of conjugation time, thereby forming an unreactive hydroxido complex HO-*Lx* (t_R = 11.2 min.). This rapid hydrolysis explains the similar results obtained for the Cl-*Lx* **1a** and Br-*Lx* **1b** complexes (Fig. S23).

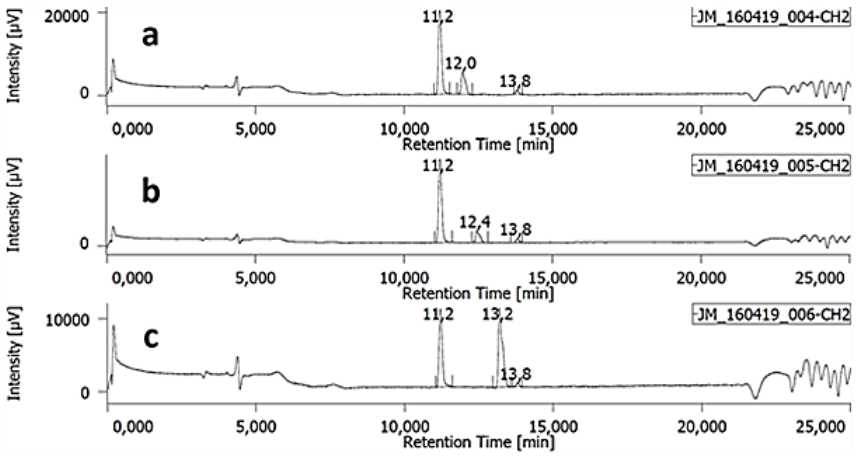

Figure S24. C18 Alltima HPLC chromatograms (at 430 nm) of the conjugation mixtures in HEPES after 1 h conjugation time in the absence of any additional salt: (**a**) Cl-*Lx* (**1a**); (**b**) Br-*Lx* (**1b**); (**c**) I-*Lx* (**1c**).

This hydrolysis effect was found to be less significant when the I-*Lx* complex **1c** was used (Fig. S24c), but also in this mixture ~50% were converted to the hydrolyzed HO-*Lx* species after 1 h conjugation time. This explains the lower reactivity when no excess of iodide – which would stabilize the reactive I-*Lx* complex **1c** – was present.

To make a fair comparison between the reactivity of the halido leaving groups, they should be stabilized during the conjugation by addition of a certain amount of a corresponding sodium halide salt. The salt concentration which was needed to keep the halido-*Lx* complex intact (*i.e.* to preserve at least 90% of the reactive complex Hal-*Lx* after 4 h conjugation time) under the conjugation conditions was determined by C18 Alltima HPLC. These results show that for the I-*Lx* complex **1c** the presence of 10 mM NaI was already sufficient (Fig. S27), the Br-*Lx* complex **1b** was found stable when 50 mM NaBr was used (Fig. S26), and for the Cl-*Lx* complex **1a** a large excess of 200 mM NaCl was required (Fig. S25).

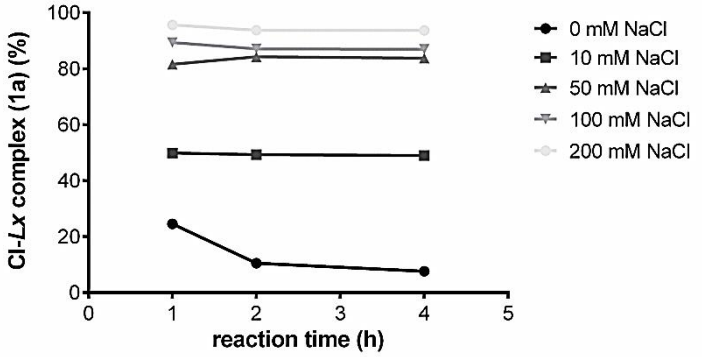

Figure S25. Stability of Cl-*Lx* (**1a**) under the conjugation conditions in the presence of different concentrations of NaCl.

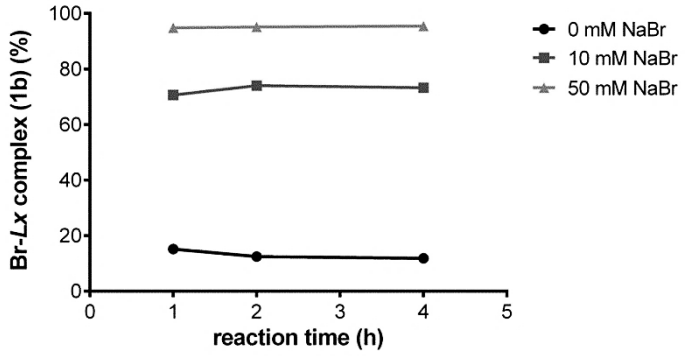

Figure S26. Stability of Br-*Lx* (**1b**) under the conjugation conditions in the presence of different concentrations of NaBr.

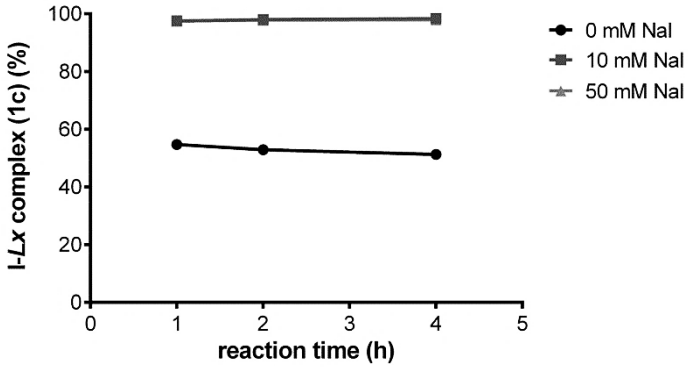

Figure S27. Stability of I-*Lx* (**1c**) under the conjugation conditions in the presence of different concentrations of NaI. *Note*: curves for 10 mM and 50 mM NaI concentrations overlap.

With these stabilizing concentrations in hands, we performed conjugations of the three halido complexes **1a**, **1b**, and **1c** similar to the conjugation experiments described in Table S24 and Fig. S23, but now with the addition of 200 mM NaCl, 50 mM NaBr, and 10 mM NaI, respectively (Fig. S28; also Fig. 5A of the main part of the manuscript).

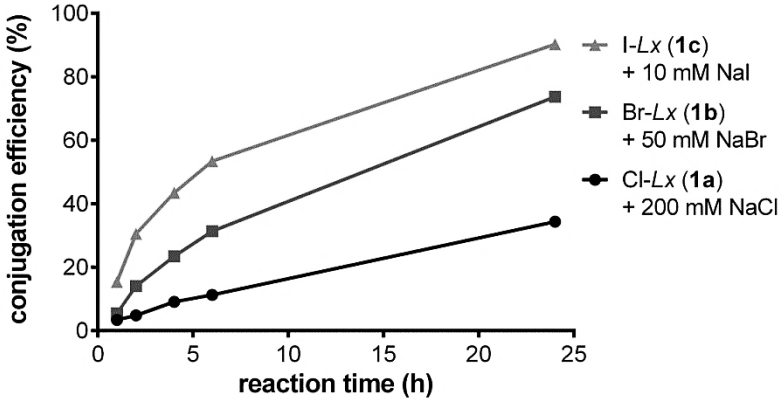

Figure S28. Conjugation efficiencies obtained in the presence of corresponding sodium salts for stabilization of the Hal-*Lx* complexes **1a-c**.

Under these conditions we obtained convincing results showing that the iodido complex I-*Lx* (**1c**) was most efficient in the conjugation (90% efficiency after 24 h conjugation time), the chlorido complex Cl-*Lx* (**1a**) was found least efficient (34% efficiency after 24 h conjugation time), and the bromido complex Br-*Lx* (**1b**)

showed an intermediate efficiency that was between that of its two halido homologs **1a** and **1c** (74% efficiency after 24 h conjugation time) but was closer to the iodido complex **1c**.
Although the applied buffer, phosphate buffered saline (PBS), contains large amounts of chloride (142 mM), it does not hamper the *Lx*-conjugation. Apparently, the addition of 10 mM NaI is sufficient to exert the iodide effect even in the presence of a large excess of chloride (~82 mM in the conjugation mixture after dilution).

3.14. Screening of the reaction molarity

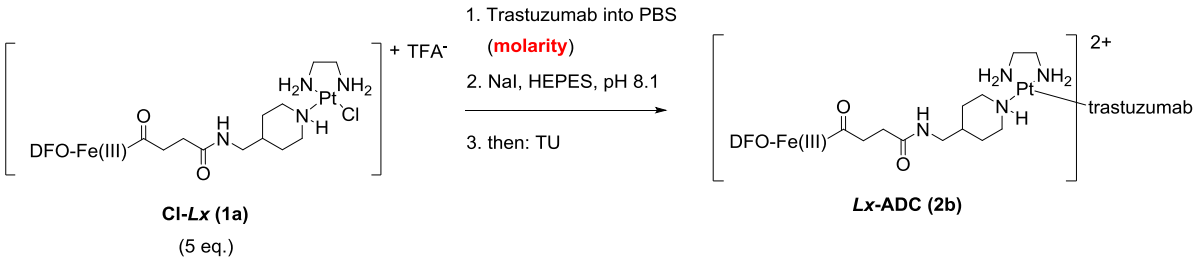

Scheme S16. Screening of the reaction molarity.

The standardly used concentration of trastuzumab in *Lx*-conjugations is 12 mg/mL. In this experiment, the effect of a higher (2 × and 4 × increase) and lower (2 × and 4 × decrease) protein concentrations was explored. To this end, the protein was buffer exchanged into PBS before it was concentrated or diluted. Note that also the concentration of the complex Cl-*Lx* (**1a**) was changed accordingly to keep the reaction stoichiometry constant (5.0 eq. of the complex **1a** were used).

Conjugation procedure: Trastuzumab, after exchange of its native clinical formulation buffer (concentration according to Table S25), and Cl-*Lx* **1a** (5 eq.) were incubated in HEPES/NaI, pH 8.1 at 47 ^{o}C. After the conjugation followed by treatment with a solution of TU, the mixtures were analyzed by SEC to determine the conjugation efficiency (Fig. S29).

Table S25. Screening of trastuzumab (and Cl-*Lx* (**1a**)) concentrations.

Entries	Buffer	Buffer concentration (mM)	Buffer pH	Additional salt in the buffer	Additional salt concentration (mM)	Eq. *Lx*	Reaction temperature (°C)	Reaction time (h)	Antibody buffer	Trastuzumab concentration (relative concentration)
349-353	HEPES	20	8.1	NaI	10	5	47	1-24	PBS	12 mg/mL (1.0)
354-358	HEPES	20	8.1	NaI	10	5	47	1-24	PBS	3 mg/mL (0.25)
359-363	HEPES	20	8.1	NaI	10	5	47	1-24	PBS	6 mg/mL (0.5)
364-368	HEPES	20	8.1	NaI	10	5	47	1-24	PBS	24 mg/mL (2.0)
369-373	HEPES	20	8.1	NaI	10	5	47	1-24	PBS	48 mg/mL (4.0)

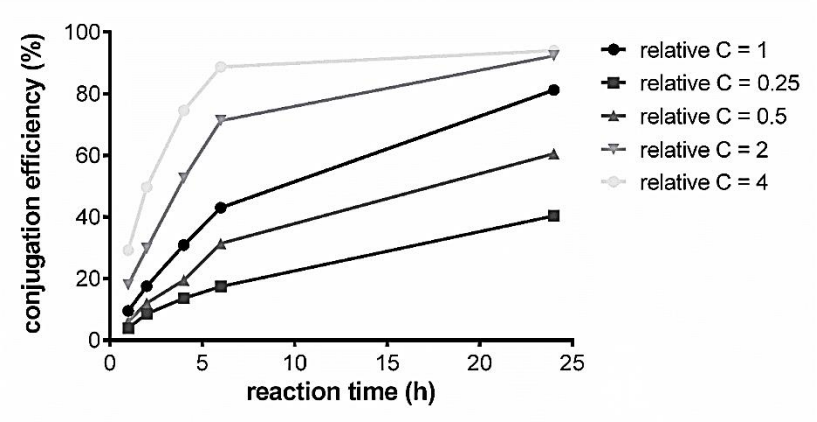

Figure S29. The effect of the antibody (and Cl-*Lx* (**1a**)) concentration on the *Lx*-conjugation efficiency. C = concentration.

Expectedly, the increase in concentration accelerated the conjugation and decrease in concentration slowed it down (Fig. S29). A plateau value of ~90% was already reached after 6 h when the concentration was 4 × increased (48 mg/mL); the same value was obtained at a 2 × increased concentration (24 mg/mL) after a longer conjugation time (24 h). Next to an increased conjugation rate, also an increase in the protein aggregation was observed (1.4%, 2.4%, and 3.4% aggregation for 12 mg/mL (entries 349-353), 24 mg/mL (entries 364-368), and 48 mg/mL (entries 369-373), respectively). Since this finding indicates a lower protein stability at a higher concentration, it was decided not to proceed with increased trastuzumab concentrations. However, depending on the chosen mAb, this parameter would need optimization in case a large scale manufacturing is envisioned.

4. Comparison of *Lx*-conjugates 2a and 2b obtained via the initial and the optimized *Lx*-conjugation procedures applied to Cl-*Lx*-DFO-Fe(III) (1a)

The optimized *Lx*-conjugation method was applied to the semi-final complex Cl-*Lx*-DFO-Fe(III) (Cl-*Lx*; (**1a**)) (Scheme S17) and the properties of the thus obtained DFO-Fe(III) based *Lx*-conjugate **2b** were compared to the properties of the *Lx*-conjugate **2a** obtained via the initial *Lx*-conjugation method.

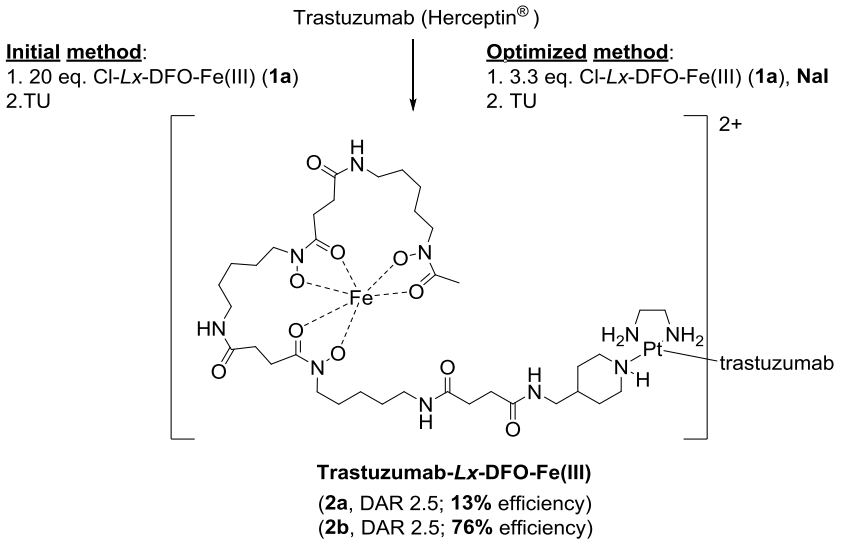

Scheme S17. Synthesis of the DFO-Fe(III) based *Lx*-conjugates **2a** and **2b**, both with DAR 2.5 (determined after the de-ironization, *vide infra*).

4.1. Synthesis of DFO based *Lx*-conjugates 2a and 2b using the initial and the optimized *Lx*-conjugation methods from Cl-*Lx*-DFO-Fe(III) (1a)

4.1.1. Milligram scale synthesis of *Lx*-conjugate 2a

The milligram scale synthesis of **2a** (via the **initial method**) was described in section 2.1. and in [1] Sijbrandi *et al.*, *Cancer Res.* **2017**, *77*, 257-267.

4.1.2. Milligram scale synthesis of *Lx*-conjugate 2b

Conjugation procedure (optimized method): In a 1.5 mL screw cap Eppendorf tube, trastuzumab in PBS (5.0 mg, 238 µL of a 21 mg/mL solution, 1.0 eq.) was diluted with 200 mM HEPES buffer containing 100 mM NaI (41.2 µL, pH 8.1; final concentrations 20 mM HEPES and 10 mM NaI), then Cl-*Lx* (**1a**) (24.1 µL of a 20 mM NaCl solution, ~3.3 eq.) and milliQ water (109.9 µL) were added. The sample was incubated in a thermoshaker at 47 °C for 24 h, followed by the addition of TU (413 µL of a 20 mM solution, final concentration 10 mM) and incubation at 37 °C for 30 min. DAR: 2.5 (as determined by SEC-MS).

De-ironization and purification of the *Lx*-conjugate **2b** (Scheme S18, 1. step): Fe(III) was removed from the DFO chelator using EDTA (incubation at 37 °C for 30 min). The product was purified by spin filtration and collected in a 0.9% NaCl solution.

The antibody integrity was not altered by modification according to the SEC analysis.

4.2. Immunoreactive antibody fraction after the *Lx*-conjugation

To obtain information about the bioconjugate properties after the *Lx*-conjugation, the immunoreactive antibody fraction of the *Lx*-conjugates obtained via the initial and the optimized methods was measured. To this end, the *Lx*-conjugates **2a** and **2b** were radiolabeled with ^{89}Zr (Scheme S18)[10], followed by LINDMO immunoreactivity assay[4] of thus obtained radiolabeled *Lx*-conjugates **^{89}Zr-2a** and **^{89}Zr-2b** (Fig. S30).

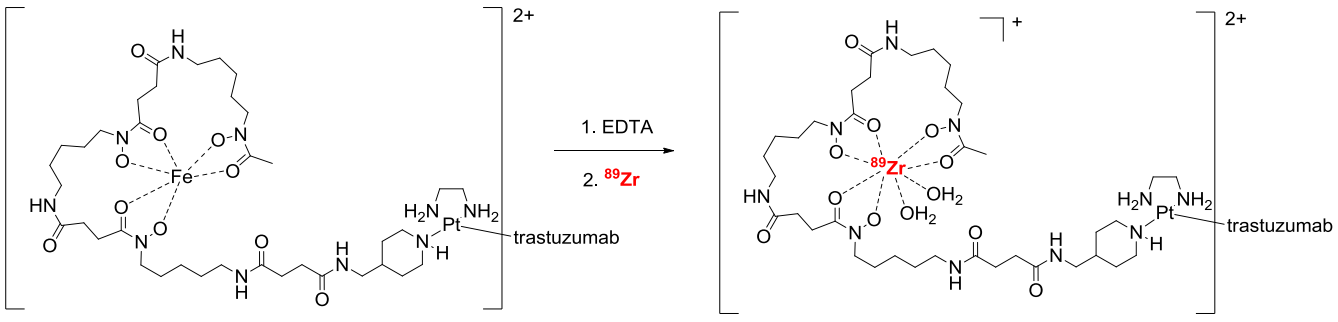

Trastuzumab-*Lx*-DFO-Fe(III)
(**2a**, DAR 2.5)
(**2b**, DAR 2.5)

Trastuzumab-*Lx*-DFO-^{89}Zr(IV)
(**^{89}Zr-2a**, DAR 2.5)
(**^{89}Zr-2b**, DAR 2.5)

Scheme S18. Radiolabeling of *Lx*-conjugates **2a** and **2b** with ^{89}Zr.

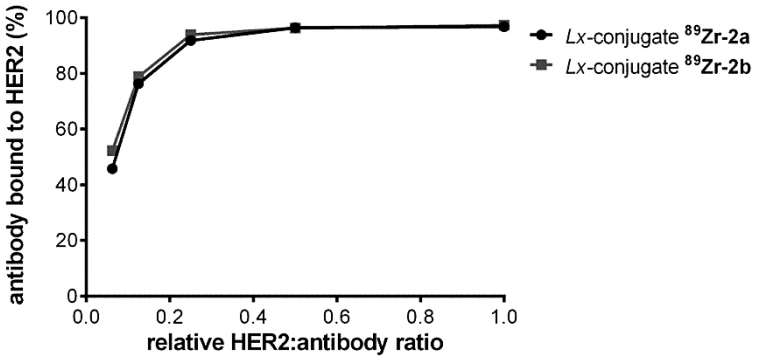

Figure S30. The LINDMO immunoreactivity assay of radiolabeled *Lx*-conjugates **^{89}Zr-2a** and **^{89}Zr-2b**.

No change in the immunoreactivity assay of the radiolabeled *Lx*-conjugates **^{89}Zr-2a** and **^{89}Zr-2b** was observed, indicating that the binding properties of the conjugates to the HER2 receptor were not altered by the optimized conjugation procedure.

4.3. Comparison of the serum stability of *Lx*-conjugates ^{89}Zr-2a and ^{89}Zr-2b

The serum stability of the two radiolabeled *Lx*-conjugates **^{89}Zr-2a** and **^{89}Zr-2b** was measured (as described in [1] Sijbrandi *et al.*, *Cancer Res.* **2017**, *77*, 257-267) and found to be unaltered (Fig. S31).

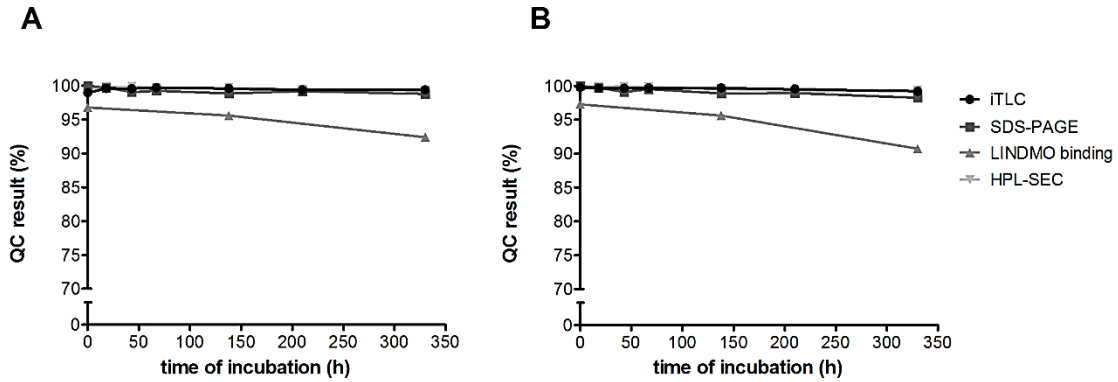

Figure S31. The serum stability experiment in human AB serum/NaCl (0.9%) with the radiolabeled *Lx*-conjugates **^{89}Zr-2a** (**A**) (prepared using the initial *Lx*-conjugation conditions) and **^{89}Zr-2b** (**B**) (prepared using the optimized *Lx*-conjugation conditions). QC = quality control.

4.4. Comparison of the pharmacokinetics of *Lx*-conjugates ^{89}Zr-2a and ^{89}Zr-2b

The biodistribution and the blood kinetics of the two radiolabeled *Lx*-conjugates **^{89}Zr-2a** and **^{89}Zr-2b** were assessed (as described in [10] Muns *et al.*, *J. Nucl. Med.* **2018**, *59*, 1146-1151) and found to be similar (Fig. S32 and Fig. S33; also Fig. 5A and 5B of the main part of the manuscript, respectively).

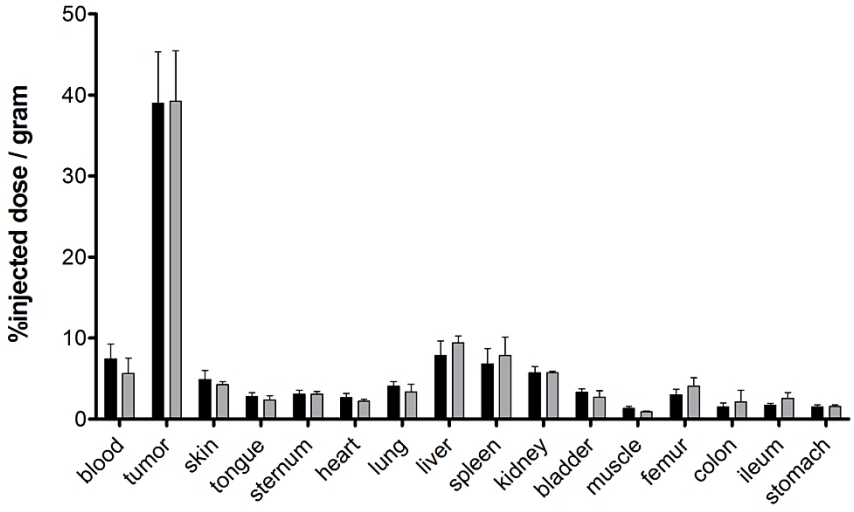

Figure S32. Biodistribution 72 h after injection of 4 mg/kg dose of radiolabeled *Lx*-conjugates **^{89}Zr-2a** (black bars; initial method) and **^{89}Zr-2b** (gray bars; optimized method) in NCI-N87 xenograft bearing mice (N = 6/group), assessed by ^{89}Zr counting. The error bars represent the standard deviation.

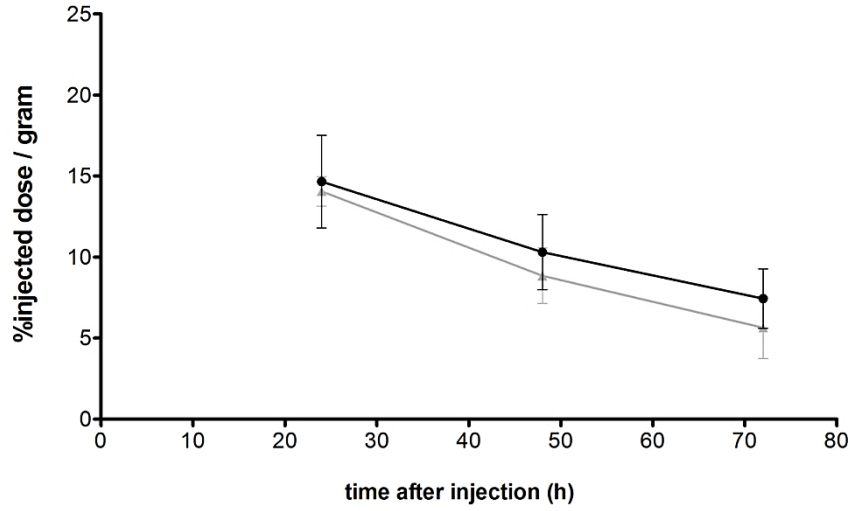

Figure S33. Blood kinetics after injection of 4 mg/kg dose of radiolabeled *Lx*-conjugates **^{89}Zr-2a** (black line; initial method) and **^{89}Zr-2b** (gray line; optimized method) in NCI-N87 xenograft bearing mice (N = 6/group), assessed by ^{89}Zr counting. The error bars represent the standard deviation.

5. Comparison of *Lx*-conjugates 3a and 3b obtained via the initial and the optimized *Lx*-conjugation procedures applied to Cl-*Lx*-AF (1f)

The optimized *Lx*-conjugation method described above has now been applied to the semi-final complex Cl-*Lx*-AF (**1f**) (Scheme S19) and the properties of the thus obtained auristatin F based *Lx*-conjugate **3b** were compared to the properties of the *Lx*-conjugate **3a** obtained via the initial *Lx*-conjugation method.

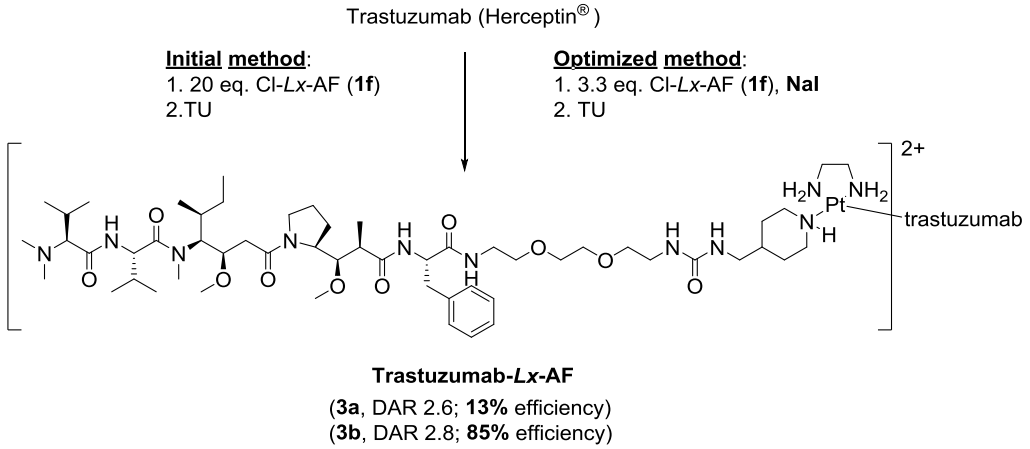

Scheme S19. Synthesis of *Lx*-conjugates **3a** and **3b** from the chlorido semi-final complex Cl-*Lx*-AF (**1f**) using the initial and the optimized *Lx*-conjugation methods, respectively.

5.1. Synthesis of auristatin F based *Lx*-conjugates 3a and 3b from Cl-*Lx*-AF (1f) using the initial and the optimized *Lx*-conjugation methods

5.1.1. Milligram scale synthesis of *Lx*-conjugate 3a

The milligram scale synthesis of the *Lx*-conjugate **3a** (via the **initial method**) was described in section 2.2. and in [1] Sijbrandi *et al.*, *Cancer Res.* **2017**, *77*, 257-267.

5.1.2. Milligram scale synthesis of *Lx*-conjugate 3b

Conjugation procedure (optimized method): In a 1.5 mL screw cap Eppendorf tube, I-*Lx*-AF (**1f**) (I-*Lx*-AF; 33.7 µL of a ~5 mM solution in water/DMA 9:1, ~3.3 eq.) and MilliQ (170.4 µL) were added to a solution of trastuzumab (Herceptin®; 7.5 mg, 357 µL of a 21 mg/mL solution in PBS, 1.0 eq.) in HEPES/NaI buffer (62.8 µL of a 200 mM HEPES and 100 mM NaI solution, pH 8.1) and incubated in the thermoshaker at 47 °C for 24 h. Then, TU (623.9 µL of a 20 mM solution; final concentration 10 mM) was added to the mixture that was incubated in the thermoshaker at 37 °C for 30 min. After that, the mixture was purified using a spin filter (MWCO = 30 kDa; 15 mL, washed 4 × with PBS buffer, reconstituted to 1.5 mL). The desired conjugate **3b** was obtained as an ~5 mg/mL solution in PBS.

5.2. Comparison of DAR and payload distribution

To determine the DAR and the payload distribution, the SEC-MS spectra of the intact (DAR determination), reduced (Hc/Lc distribution), papain digested (Fab/Fc distribution), and pepsin digested ($F(ab')_2$ distribution) *Lx*-conjugates **3a** (obtained via the initial method) and **3b** (obtained via the optimized method) were compared, as described in [1] N. J. Sijbrandi *et al.*, *Cancer Res.* **2017**, *77*, 257-267.

SEC-MS analysis of the *Lx*-conjugate **3a** (**initial method**): DAR 2.55 (conjugation efficiency: **13%**); %Hc = 90%, %Lc = 10%, %$F(ab')_2$ = 15%, %Fab = 13%, %Fc = 87%.

SEC-MS analysis of the *Lx*-conjugate **3b** (**optimized method**): DAR = 2.81 (conjugation efficiency: **85%**), %Hc = 87%, %Lc = 13%, %$F(ab')_2$ = 22%, %Fab = 15%, %Fc = 85%.

5.3. *In vitro* efficacy of auristatin F based *Lx*-conjugates 3a and 3b

The obtained *Lx*-conjugates **3a** and **3b** were tested in CTB assays on three HER2 positive cancer cell lines: NCI-N87, SK-OV-3, and JIMT-1 (Fig. S34; also Fig. 6 of the main part of the manuscript for JIMT-1).

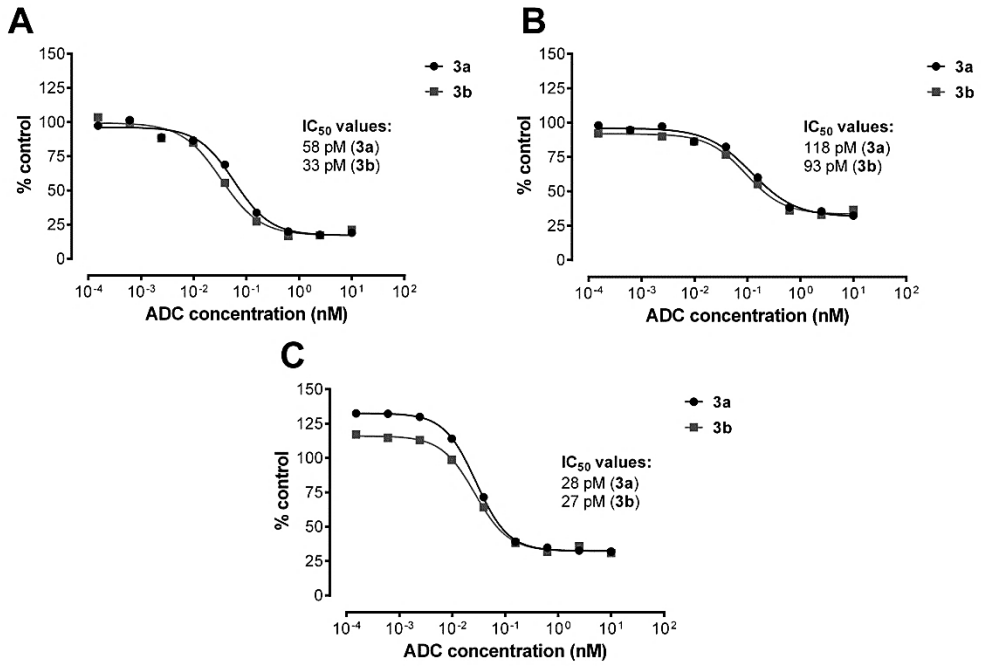

Figure S34. Results of CTB assays in HER2 positive cell lines NCI-N87 (**A**), SK-OV-3 (**B**), and JIMT-1 (**C**) with trastuzumab-*Lx*-AF synthesized under the optimized conditions (**3b**) and the initial conditions (**3a**).

We obtained similar cell toxicity results (*i.e.* similar IC_{50} values in the pM range for both conjugates **3b** and **3a**) supporting our hypothesis that the optimized *Lx*-conjugation method does not alter the properties of the *Lx*-conjugates. The *Lx*-conjugates also showed no toxicity on the HER2 negative cell line MDA-MB-231 (data not shown), indicating that no free toxin is present.

6. The formulation stability study of the lead *Lx*-ADC trastuzumab-*Lx*-AF ($3b_{stab}$)

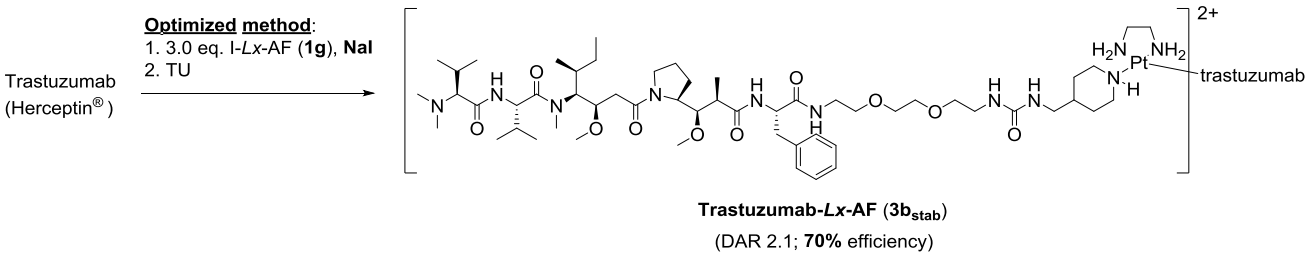

Scheme S20. Synthesis of *Lx*-conjugate $\mathbf{3b_{stab}}$ for the stability study from the iodido semi-final complex I-*Lx*-AF (**1g**) using the optimized *Lx*-conjugation method.

The multigram scale synthesis and analytical characterization of the lyophilizate I-*Lx*-AF (**1g**) × 2.0 TFA × 2.5 NaI was described in [2] E. Merkul *et al.*, *Green Chem.* **2020**, *22*, 2203-2212.

6.1. The conjugation procedure, formulation, and storage conditions

Conjugation procedure (optimized method): Trastuzumab (Herceptin®; 60 mg, 2.86 mL of a 21 mg/mL solution, 1.0 eq.), buffer exchanged into PBS, was diluted with 200 mM HEPES buffer containing 100 mM NaI (494 µL, pH 8.1; final concentrations 20 mM HEPES and 10 mM NaI), then I-*Lx*-AF (**1g**) (237.6 µL of a ~5 mM solution in water/DMA 9:1, ~3.0 eq.) was added, followed by addition of milliQ water (1.35 mL). The mixture was incubated in a thermoshaker at 47 ^{o}C for 24 h, followed by the addition of TU (548 µL of a 100 mM solution; final concentration 10 mM) and incubation at 37 ^{o}C for 30 min. The conjugate was then purified by spin filtration using 30 kDa MWCO filters (15 mL volume; washed 4 × with the Herceptin® formulation buffer), after which it was reconstituted to 12 mL. The product trastuzumab-*Lx*-AF (**3b$_{stab}$**) was sterile filtered using a Minisart® NML Syringe Filter (type 16534). DAR: 2.1 (as determined by SEC-MS).

The product **3b$_{stab}$** was formulated as 5 mg/mL solution (60 mg scale, 12 mL of the formulation) in the Herceptin® formulation buffer. The formulated solution was aliquoted into Eppendorf vials (40 × 300 µL) before storage. Half of the aliquoted fractions was lyophilized before storage. The lyophilization was performed using a lyophilizer (Christ; Alpha 2-4 LDplus 101542; Serial No. 23344).

Both the lyophilized powder and the solution were stored (time point zero) at -18 °C (the freezer (Liebherr; LCv 4010; Serial No. 9997597-01) was not centrally monitored but an alarm (beeper) limit was set at -16 °C) and at room temperature (defined as 21 ^{o}C +/- 5 ^{o}C), after which samples were taken and analyzed at different time points during the course of one year.

6.2. The stability study

The stability of the *Lx*-ADC during the course of one year was assessed by measuring several critical quality attributes (CQAs) according to a schedule (Table S26). Lyophilized trastuzumab-*Lx*-AF (**3b$_{stab}$**) was reconstituted by the addition of 300 µL WFI (Water for Injection). Analysis was executed within 2 days after thawing of the samples.

Table S26. Stability study schedule.

CQA [method]	D 1 (1 day)	D 7 (1 week)	D 28	D 30 (1 month)	D 92 (3 months)	D 124	D 183 (6 months)	D 194	D 365 (1 year)
Protein content [UV]	X	X	-	X	X	-	X	-	X
Monomeric purity [SEC]	X	X	-	X	X	-	X	-	X
Protein composition [SDS-PAGE]	X	X	-	X	X	-	X	-	X
Potency in HER2 positive cell lines [CTB][a]	X	X	-	X	X	-	X	-	X
DAR [SEC-MS]	X	X	**X***	X	X	**X***	X	**X***	X

X: sample taken and analyzed
X*: additional samples taken for DAR assessment
[a] assessed in NCI-N87, SK-OV-3, JIMT-1, and BT-474. MDA-MB-231 was used as a HER2 negative control cell line

The results of the formulation study are summarized in Table S27.

Table S27. Results of the formulation stability study of trastuzumab-*Lx*-AF (**3b$_{stab}$**).

Time point	Lyophilized; -18 °C	Solution; -18 °C	Lyophilized; RT	Solution; RT
1 day	no change	no change	no change	no change
1 week	no change	no change	no change	no change
1 month	no change	no change	no change	no change
3 months	no change	no change	no change	no change
6 months	no change	no change	no change	no change
1 year	no change	no change	change (potency, DAR)	change (potency, DAR)

It was found that our ADC product was stable for at least one year at -18 ^{o}C (intended storage condition) and for at least six months at room temperature (RT; accelerated storage condition), both in solution and as a lyophilizate.

7. The multigram scale synthesis of the lead *Lx*-ADC trastuzumab-*Lx*-AF (3c) from I-*Lx*-AF (1g) using the optimized *Lx*-conjugation procedure

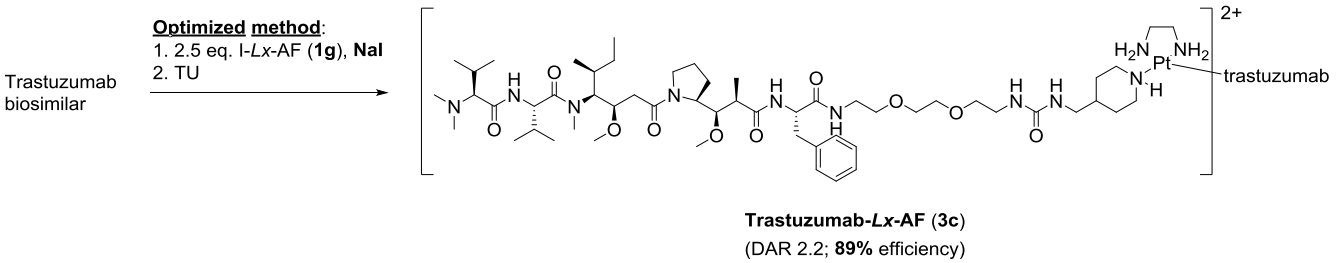

Scheme S21. The multigram synthesis of trastuzumab-*Lx*-AF (**3c**) from I-*Lx*-AF (**1g**) using the optimized *Lx*-conjugation method.

7.1. The multigram scale synthesis of the semi-final complex I-*Lx*-AF (1g)

The multigram scale synthesis and analytical characterization of the lyophilizate I-*Lx*-AF (**1g**) × 2.0 TFA × 2.5 NaI was described in [2] E. Merkul *et al.*, *Green Chem.* **2020**, *22*, 2203-2212. This material was used for the multigram *Lx*-ADC synthesis described in section 7.2.

7.2. The multigram scale synthesis of trastuzumab-*Lx*-AF (3c) from I-*Lx*-AF (1g) using the optimized *Lx*-conjugation method

7.2.1. The multigram scale *Lx*-conjugation procedure

The conjugation mixture was prepared as outlined in Table S28.

Conjugation procedure (optimized method): Trastuzumab BS (5.1 g; 130.435 mL, 39.3 mg/mL, defined as 1.0 eq.) was diluted with PBS (26.8 mL), then 200 mM HEPES buffer containing 100 mM of NaI solution (27.2 mL, pH 8.1) was added, followed by the addition of a solution of I-*Lx*-AF (**1g**) (16.8 mL, ~5 mM in water/DMA 9:1, ~2.5 eq.) and MilliQ water (71.7 mL). Mixing of all components resulted in a clear and colorless mixture.

In 5-fold, 413 µL of the resulting solution were transferred to 1.5 mL Eppendorf tubes and used as control small scale conjugations (section 7.2.3.).

The final concentrations of HEPES and NaI were 20 mM and 10 mM, respectively; the final concentrations of I-*Lx*-AF (**1g**) and trastuzumab BS were 307 µM and 126 µM, respectively, corresponding to a molar ratio of I-*Lx*-AF (**1g**) to trastuzumab BS of 2.45. The pH of the conjugation mixture was measured at start of the incubation and after the incubation.

The conjugation mixture was incubated in an oil bath at 47 °C for 24 h using a magnetic stirring bar. No change in pH was observed between start and end of the conjugation reaction (pH_{start} = 7.83; pH_{end} = 7.81).

Table S28. The multigram scale *Lx*-conjugation mixture.

Step	Added component	Added volume (mL)	Cumulative volume (mL)	Concentration of trastuzumab BS (µM)	Concentration of I-*Lx*-AF (1g) (µM)
1	Trastuzumab BS (39.3 mg/mL)	130.4	130.4	264	0
2	PBS	26.8	157.2	219	0
3	HEPES/NaI, pH 8.1 (200/100 mM)	27.2	184.4	186	0
4	I-*Lx*-AF (**1g**) (5.0 mM)	16.8	201.2	171	417
5	MilliQ	71.7	272.9	126	307

7.2.2. Quenching with TU

Following incubation, the TU solution was added (30 mL, 100 mM in H_2O; final concentration was 10 mM), and the mixture was incubated in the oil bath at 47 °C for another 30 min. The mixture was then allowed to cool to room temperature before the diafiltration was performed.

7.2.3. Purification by diafiltration

The multigram scale product **3c** was purified by Hollow Fiber Tangetial Flow Filtration (TFF; diafiltration). The diafiltration setup consisted of a peristaltic pump (Watson Marlow 520u), a pressure monitor (PressureMAT™; PendoTECH) including corresponding pressure sensors and a Minikros Sampler Hollow Fiber Filter Module (Repligen; Product No: S02-E030-05-N; LOT No: 3311583-05/19-008).

During the diafiltration procedure, pressure and flow rates were constantly monitored. The pressure on the column's inlet tube (P_{in}), on the column's outlet tube (P_{ret}), and on the column's permeate tube (P_{perm}) were monitored, as well as the volume increase in the permeate over time. The monitored pressures were used to calculate the transmembrane pressure (TMP) in bar, which was defined as $TMP = ((P_{in} + P_{ret})/2) - P_{perm}$. The permeate volume increase over time was used to calculate the flux (LMH), which is defined as volume (L) per hollow fiber area (m^2) per hour (h). Both TMP and flux are of importance when upscaling or downscaling the process. The TMP and LMH values during the diafiltration process are shown in Fig. S35.

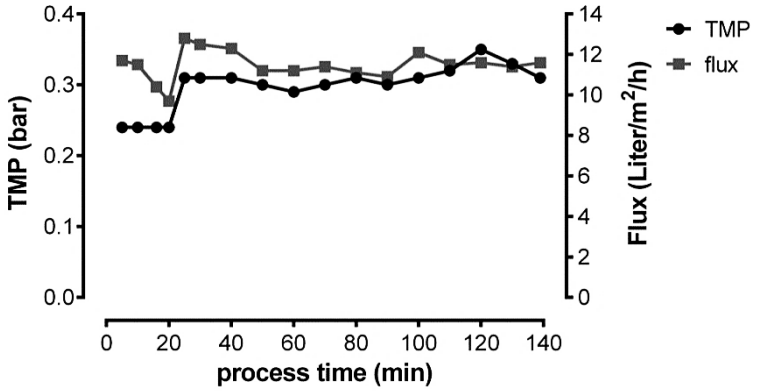

Figure S35. In-process monitoring of TMP and flux during the diafiltration.

The reaction mixture volume was constant (~300 mL) during the full diafiltration process. The process was stopped when the volume in the permeate reservoir reached 2.1 L. This volume corresponds to 7 × of the reaction mixture's volume, which is known to be sufficient for a complete buffer exchange and purification. After diafiltration, the product volume was reconstituted to ~660 mL by addition of the Herceptin® formulation buffer, which resulted in the multigram scale batch **3c** in the desired concentration of ~5 mg/mL.
This batch of trastuzumab-*Lx*-AF (**3c**) was generated only for validation purposes of the newly developed *Lx*-conjugation method.

7.3. Quality control (QC) of trastuzumab-*Lx*-AF (3c) produced on a multigram scale using the optimized *Lx*-conjugation method

The products A-E (**3c$_{ref}$**) obtained from the milligram scale control *Lx*-conjugation reactions using the same conjugation mixture as for the multigram scale synthesis of **3c** were used as references in these QC determinations. They were prepared using the optimized *Lx*-conjugation conditions.

Table S29 summarizes the QC results of the multigram scale batch of trastuzumab-*Lx*-AF (**3c**).

Table S29. QC results.

QC attribute [method]	Multigram scale conjugate 3c	Milligram scale control conjugates 3c$_{ref}$
Protein content [UV][a]	5.3 mg/mL	5.6 mg/mL
Monomeric purity [SEC][b]	96.1%	95.2%
Protein composition [SDS-PAGE]	Similar to parental mAb	Similar to parental mAb
TU-*Lx*-AF (1h) [HPLC]	<LOD	<LOD
DAR [SEC-MS]	2.2	2.3
Potency in HER2 positive cell lines [CTB][c]	Subnanomolar	Subnanomolar

[a] The anticipated protein concentration was 5.0 mg/mL

[b] BS had a monomeric purity of 95.7%

[c] No potency (IC_{50} > 1000 nM) was observed in MDA-MB-231 (HER2 negative control cell line)

7.3.1. Protein content by Nanodrop UV

Calculated concentrations are listed in Table S30.

Table S30. Determined protein concentrations.

Sample	Concentration of 3c/$3c_{ref}$ (mg/mL)[a]	Concentration of 3c/$3c_{ref}$ (µM)[b]
Multigram scale conjugation product (3c)	5.3	36.5
Reference product A ($3c_{ref}$)	5.6	38.4
Reference product B ($3c_{ref}$)	5.5	38.1
Reference product C ($3c_{ref}$)	5.4	37.4
Reference product D ($3c_{ref}$)	5.8	39.6
Reference product E ($3c_{ref}$)	5.6	38.8

[a] Triplicate measurements

[b] Conjugate **3c**/**$3c_{ref}$** molecular weight used for calculations = 145000 Da

7.3.2. Monomeric purity by SEC

The monomeric purity (*i.e.* monomeric fraction) was calculated from the SEC chromatograms as the area of the peak representing the monomeric form (with t_R ~7.3 min., Fig. S36) relative to the total area of all peaks (*i.e.* including the multimeric or aggregate peak at t_R ~6.4 min.).

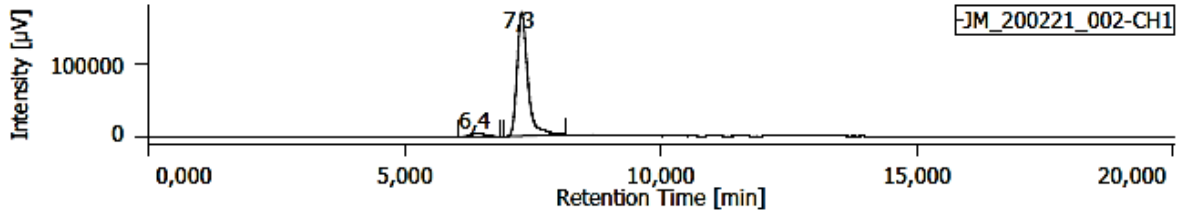

Figure S36. Chromatogram (SEC trace) of the formulated multigram scale product **3c**, showing monomeric fraction at t_R = 7.3 min. and oligomeric fraction at t_R = 6.4 min.

The monomeric purity was high and constant (>95%; the used BS had a monomeric purity of 95.7%) in the multigram scale product **3c** as well as in the reference products **$3c_{ref}$** (Table S31). It should be mentioned that the decrease in monomeric purity of the reference products when compared to the multigram scale product is minor, but consistent, which might be due to temporarily high product concentrations when purification is performed by spin filtration, and therefore is considered to be a positive effect of upscaling.

Table S31. Monomeric purity determined by SEC.

Sample	Monomeric purity (%)	N[a]
Multigram scale conjugation product (3c)	96.1	2
Reference product A ($3c_{ref}$)	95.8	1
Reference product B ($3c_{ref}$)	95.0	1
Reference product C ($3c_{ref}$)	95.3	1
Reference product D ($3c_{ref}$)	95.2	1
Reference product E ($3c_{ref}$)	94.8	1
Mean value of reference products A-E ($3c_{ref}$)	95.2	-

[a] Number of measurements

7.3.3. Protein composition by SDS-PAGE

The protein composition of all samples was apparently identical to the protein composition of trastuzumab controls. Neither fragments nor aggregates were observed in any of the product **3c** samples compared to the controls **$3c_{ref}$**.

7.3.4. Unbound TU-*Lx*-AF (1h) by HPLC

Unbound AF is considered to be the most troublesome impurity in the final products because of its potential cytotoxicity. Since the *Lx*-AF bond is considered to be uncleavable and the conjugation reaction was quenched with TU (which shows strong affinity for Pt(II) complexes and therefore quenches the excessive precursor semi-final complex **1g**), the unbound "free" AF is considered to be present in the form of the inactivated impurity TU-*Lx*-AF (**1h**). This compound was previously shown to be 10^2 to 10^3 times less toxic compared to a similar Mal containing compound.[1]

To determine the method's limit of detection (LOD) and to quantify the amount of TU-*Lx*-AF **1h** in analyzed samples, a range of calibration standards containing TU-*Lx*-AF (**1h**) were prepared and analyzed on C18 Alltima HPLC (210 nm readout; linear gradient 20% B in A → 100% B in A in 20 min.; A = H_2O/0.1% TFA, B = MeCN/0.1% TFA). A typical example is depicted in Fig. S37. From the calibration curve, the LOD was determined to be 1 µM, which corresponds to ~1.2% of unbound AF *vs* total AF in formulated **3c** samples (considering a 5 mg/mL **3c** solution with DAR 2.5 and injection of undiluted sample).

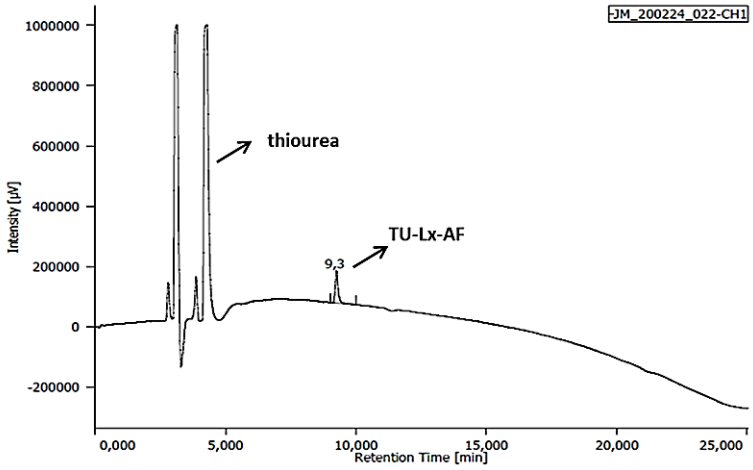

Figure S37. TU-*Lx*-AF (**1h**) calibrator solution (33.3 µM) on C18 Alltima HPLC.

The protein was removed from the sample by spin filtration (30 kDa MWCO filter) or by MeCN precipitation (addition of 2 volumes of MeCN to one volume of sample). The concentration of unbound TU-*Lx*-AF (**1h**) (formed after the quenching step with TU) was determined by injection of 20 µL sample (filtrate or supernatant) on C18 Alltima HPLC. A 20 µL sample from the permeate reservoir was injected to estimate the conjugation efficiency by comparing the determined concentration of TU-*Lx*-AF (**1h**) with the calculated theoretical maximum value. The five conjugates obtained from the milligram scale conjugation reactions were used as a reference.

In all measured samples from the multigram scale synthesis product **3c** and the reference constructs A-E (**3c$_{ref}$**), the concentration of TU-*Lx*-AF (**1h**) was <1 µM (determined LOD), and therefore could not be accurately quantified. This indicates that an efficient purification process for the multigram scale synthesis (diafiltration) as well as the reference conjugations (spin filtration) could be achieved. No unexpected peaks appeared in any of the samples, indicating that presence of unexpected small molecule AF containing impurities is unlikely.

Since the multigram scale synthesis of **3c** was performed using the optimized conjugation method, the conjugation efficiency was expected to be in the range of 80-90% (as an outcome of the optimization

described in section 3.). To determine the obtained conjugation efficiency, a sample of the permeate solution was analyzed by HPLC in triplicate to estimate the amount of unconjugated AF.

It was found that the permeate solution contained ~2.28 µM TU-*Lx*-AF (**1h**); multiplication with the total permeate volume (2.1 L) resulted in ~4.8 µmol of unconjugated AF. Since the used I-*Lx*-AF (**1g**) stock solution concentration was ~5 mM and the added volume was 16.825 mL, the total amount of AF added to the multigram scale conjugation reaction was ~84.1 µmol. Based on this calculation, ~94% of the added AF solution was conjugated to trastuzumab. It should be noted that multiple unidentified peaks appeared in the permeate solution which could contain AF. Therefore, the determined conjugation efficiency of 89% (section 7.3.7.) corresponds quite well with this overestimated value of ~94% which is calculated only based on presence of TU-*Lx*-AF (**1h**) in the permeate.

7.3.5. DAR by SEC-MS

For each sample, the average DAR was then calculated from the relative abundance of the individual DAR species present in the deconvoluted mass spectrograms, performed in triplicate for the multigram scale product **3c** and in duplicate for the reference milligram scale products **3c$_{ref}$** (A-E). The mass spectrograms of the multigram scale samples are shown in Fig. S38; all results are listed in Table S32.

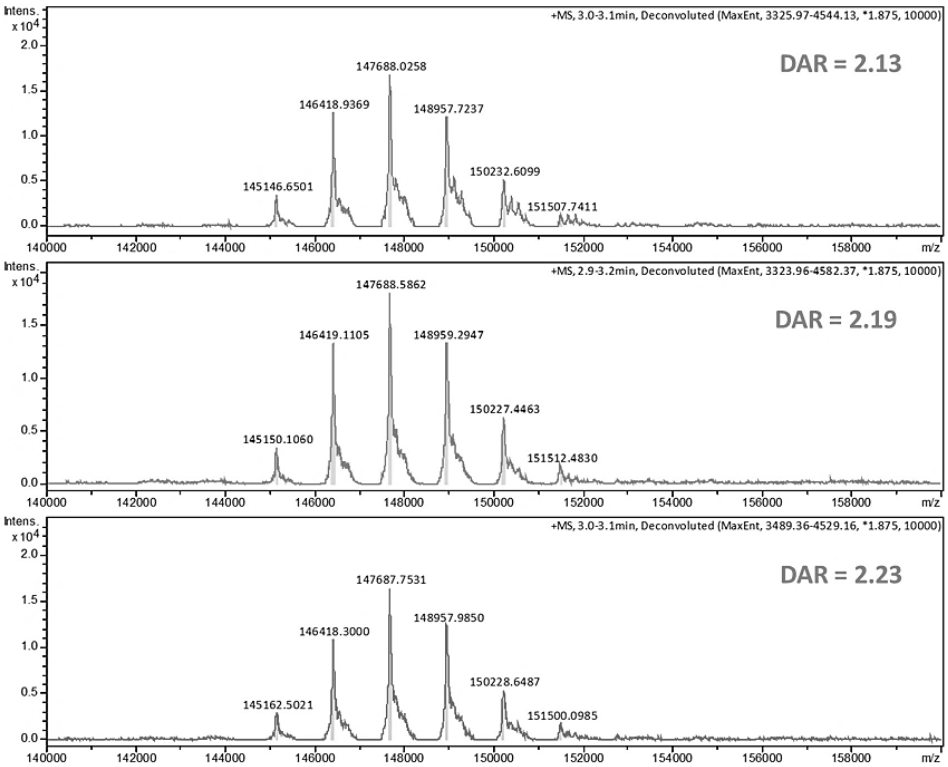

Figure S38. SEC-MS chromatograms of the multigram scale product **3c**.

Table S32. Determined DAR.

Sample	DAR	N[a]
Multigram scale conjugation product (3c)	2.2	3
Reference product A (3c$_{ref}$)	2.3	2
Reference product B (3c$_{ref}$)	2.3	2
Reference product C (3c$_{ref}$)	2.3	2
Reference product D (3c$_{ref}$)	2.3	2
Reference product E (3c$_{ref}$)	2.3	2

[a] Number of measurements

The average DAR of the multigram scale **3c** batch measurements was 2.2 (triplicate measurement); the average DAR of the reference products **3c$_{ref}$** was slightly higher (2.3).

7.3.6. Potency by CTB-based bioassay

In this assay, the multigram scale synthesis product **3c** and the reference product A (**3c$_{ref}$**) were tested. To assess potency, for each test item, the dilution series was plated across four HER2 positive reporter cell lines (NCI-N87, SK-OV-3, JIMT-1, and SK-BR-3) and one control cell line considered to be HER2 negative (MDA-MB-231), to assess non-HER2 mediated toxicity. Valid IC_{50} assessments could be made in all reporter cell lines. All samples returned IC_{50} values in the lower nanomolar range and no significant difference was observed between the multigram scale conjugation product **3c** and the reference product A (**3c$_{ref}$**) (Fig. S39, Table S33).

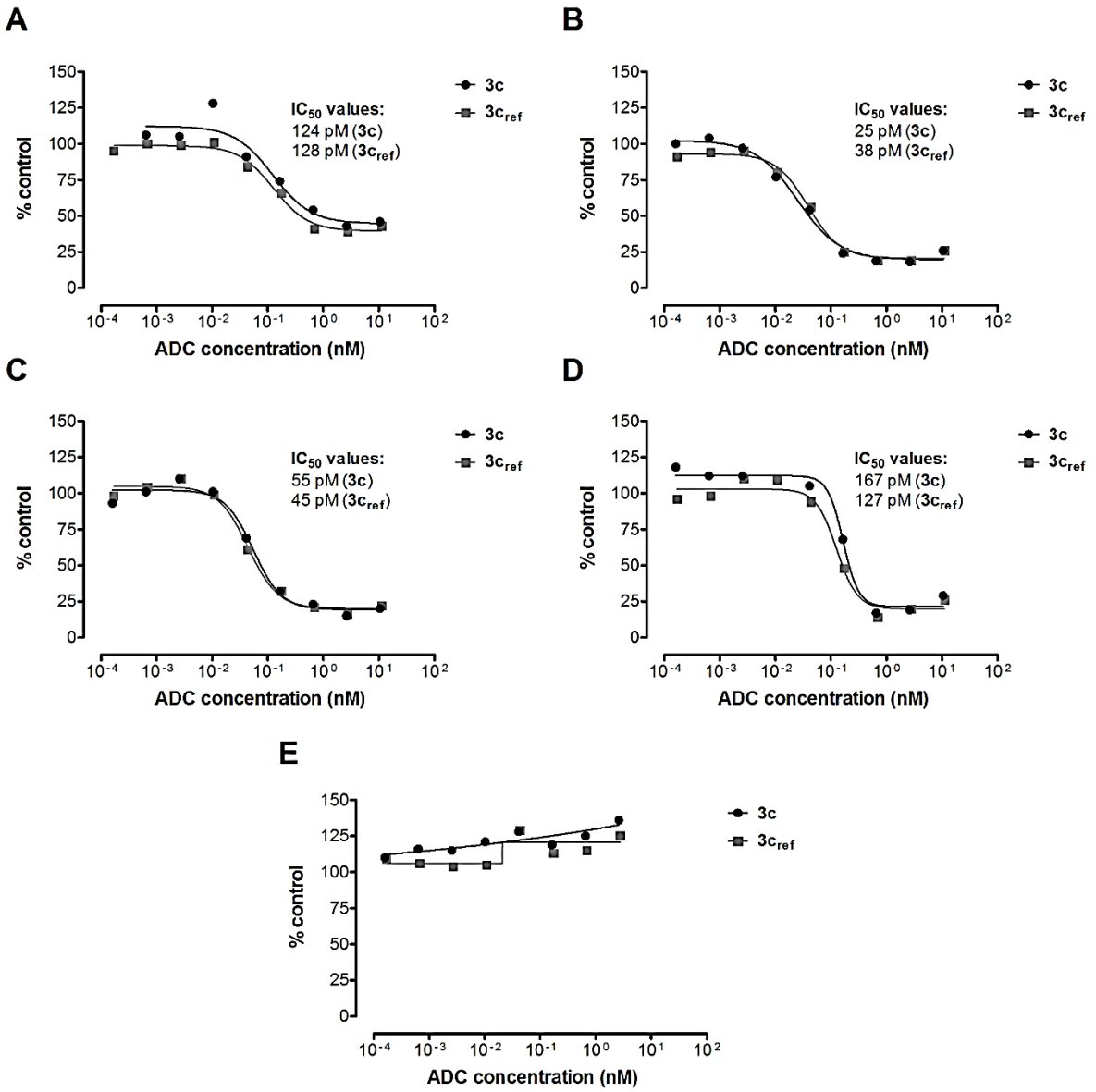

Figure S39. Results of the CTB assays in HER2 positive cell lines NCI-N87 (**A**), SK-OV-3 (**B**), JIMT-1 (**C**), and SK-BR-3 (**D**) with trastuzumab-*Lx*-AF: the multigram scale product (**3c**) compared with the milligram scale reference product A (**3c$_{ref}$**).

Table S33. IC_{50} values in pM calculated from the CTB-based bioassay.

Sample	IC_{50} in NCI-N87 cells (pM)	IC_{50} in SK-OV-3 cells (pM)	IC_{50} in JIMT-1 cells (pM)	IC_{50} in SK-BR-3 cells (pM)	IC_{50} in MDA-MB-231 cells (nM)
Multigram scale conjugation product (3c)	123.6	25.1	55.3	166.6	>1000
Reference product A ($3c_{ref}$)	127.7	38.7	44.5	127.1	>1000

8. References

1. N. J. Sijbrandi, E. Merkul, J. A. Muns, D. C. J. Waalboer, K. Adamzek, M. Bolijn, V. Montserrat, G. W. Somsen, R. Haselberg, P. J. G. M. Steverink, H.-J. Houthoff, and G. A. M. S. van Dongen. A Novel Platinum(II)–Based Bifunctional ADC Linker Benchmarked Using ^{89}Zr-Desferal and Auristatin F–Conjugated Trastuzumab. *Cancer Res.* **2017**, *77*, 257-267.
2. E. Merkul, N. J. Sijbrandi, I. Aydin, J. A. Muns, R. J. R. W. Peters, P. Laarhoven, H.-J. Houthoff, and G. A. M. S van Dongen. A successful search for new, efficient, and silver-free manufacturing processes for key platinum(II) intermediates applied in antibody-drug conjugate (ADC) production. *Green Chem.* **2020**, *22*, 2203-2212.
3. M. Tanner, A. I. Kapanen, T. Junttila, O. Raheem, S. Grenman, J. Elo, K. Elenius, J. Isola. Characterization of a novel cell line established from a patient with Herceptin-resistant breast cancer. *Mol. Cancer Ther.* **2004**, *3*, 1585-1592.
4. T. Lindmo, E. Boven, F. Cuttitta, J. Fedorko, P. Bunn. Determination of the immunoreactive function of radiolabeled monoclonal antibodies by linear extrapolation to binding at infinite antigen excess. *J. Immunol. Methods* **1984**, *72*, 77-89.
5. K. Alfonsi, J. Colberg, P. J. Dunn, T. Fevig, S. Jennings, T. A. Johnson, H. P. Kleine, C. Knight, M. A. Nagy, D. A. Perry, and M. Stefaniak. Green Chemistry Tools to Influence a Medicinal Chemistry and Research Chemistry Based Organisation. *Green Chem.* **2008**, *10*, 31-36.
6. M. Tobiszewski, S. Tsakovski, V. Simeonov, J. Namieśnik, and F. A. Pena-Pereira. Solvent Selection Guide Based on Chemometrics and Multicriteria Decision Analysis. *Green Chem.* **2015**, *17*, 4773-4785.
7. (a) J. Josephsen. Diaminehalogenoplatinum(II) Complex Reactions with DMSO. *Inorganica Chim. Acta* **2018**, *478*, 54; (b) M. D. Hall, K. A. Telma, K.-E. Chang, T. D. Lee, J. P. Madigan, J. R. Lloyd, I. S. Goldlust, J. D. Hoeschele, and M. M. Gottesman. Say No to DMSO: Dimethylsulfoxide Inactivates Cisplatin, Carboplatin, and Other Platinum Complexes. *Cancer Res.* **2014**, *74*, 3913-3922.
8. G. A. M. S. van Dongen, N. J. Sijbrandi, D. C. J. Waalboer, H.-J. Houthoff. Methods for removing weakly bound functional moieties from cell targeting conjugates. WO 2016/144171 A1, September 15, **2016**.
9. I. Berger, A. A. Nazarov, C. G. Hartinger, M. Groessl, S.-M. Valiahdi, M. A. Jakupec, B. K. Keppler. A glucose derivative as natural alternative to the cyclohexane-1,2-diamine ligand in the anticancer drug oxaliplatin? *ChemMedChem* **2007**, *2*, 505-514.
10. J. A. Muns, V. Montserrat, H.-J. Houthoff, K. Codée-van der Schilden, O. Zwaagstra, N. J. Sijbrandi, E. Merkul, G. A. M. S. van Dongen. In Vivo Characterization of Platinum(II)-Based Linker Technology for the Development of Antibody–Drug Conjugates: Taking Advantage of Dual Labeling with ^{195m}Pt and ^{89}Zr. *J. Nucl. Med.* **2018**, *59*, 1146-1151.